Research Paper

GEOSPHERE

GEOSPHERE; v. 13, no. 4

doi:10.1130/GES01351.1

8 figures; 3 tables; 2 supplemental files

CORRESPONDENCE: tjbanik@ilstu.edu

CITATION: Banik, T.J., Coble, M.A., and Miller, C.F., 2017, Porphyry Cu formation in the middle Jurassic Yerington batholith, Nevada, USA: Constraints from laser Raman, trace element, U-Pb age, and oxygen isotope analyses of zircon: Geosphere, v. 13, no. 4, doi:10.1130/GES01351.1.

Received 28 April 2016
Revision received 15 February 2017
Accepted 12 April 2017



# Porphyry Cu formation in the middle Jurassic Yerington batholith, Nevada, USA: Constraints from laser Raman, trace element, U-Pb age, and oxygen isotope analyses of zircon

**Tenley J. Banik[1,*], Matthew A. Coble[2], and Calvin F. Miller[1]**

[1]Department of Earth and Environmental Sciences, Vanderbilt University, Nashville, Tennessee 37240, USA
[2]Department of Geological Sciences, Stanford University, Stanford, California 94305, USA

## ABSTRACT

**Porphyry copper systems provide the majority of global copper resources and are generally formed from highly oxidized magmas. Zircon, a common accessory mineral in granitoid rocks that host porphyry deposits, is well established as an effective tool for assessing timescales and evolution of magmatic conditions. We present new U-Pb ages, trace element concentrations, and oxygen isotope ratios of zircon measured by secondary ion mass spectrometry (SIMS) from a suite of cogenetic host rocks and ore-bearing porphyry dikes from the Yerington copper mine, western Nevada, USA. Zircons were subjected to chemical abrasion and thermal annealing in order to evaluate Pb loss, and laser Raman analyses were performed to avoid measurements of radiation damaged or non-crystalline (potentially metamict) portions of zircon. Weighted-mean U-Pb ages from ore-bearing Yerington porphyry dikes and granitoid host plutons overlap at 2σ uncertainty, ranging from 168.7 ± 1.1 Ma to 170.0 ± 1.4 Ma. Zircon trace element concentrations show fractional crystallization trends, such as decreasing Ti versus increasing Eu anomaly ($Eu_N/Eu_N^*$) and Yb/Gd. Uranium concentrations range from 90 to 2200 ppm (average is ~320 ppm U), Eu-anomaly ratios range from 0.19 to 1.05, and $Ce_N/Ce_N^*$ values range from 20 to 980. Oxygen isotope compositions range from 4.8 ± 0.7‰ to 5.7 ± 0.8‰ (sample means), with the most depleted composition from the youngest porphyry dike. We find no statistically significant difference in ages, trace elements, or oxygen isotopes from chemically abraded and untreated zircons. Based on variations in magmatic conditions as suggested by Eu anomalies, trace element trends, model zircon crystallization temperatures, and $\delta^{18}O$ in zircon, we conclude that variable but increasing oxidation and ongoing fractional crystallization were strong controls on elemental partitioning and ore-forming processes in the Yerington system.**

*Present address: Department of Geography-Geology, Illinois State University, Normal, Illinois 61790-4400, USA

## INTRODUCTION

Zircon ($ZrSiO_4$), a common accessory mineral in silicic igneous rocks, has proven to be a versatile recorder of magmatic histories and processes. Uranium and other tetravalent elements readily substitute for Zr in zircon, while initial $Pb^{2+}$ is excluded. Together with extremely low diffusivity of Pb at magmatic temperatures (Cherniak and Watson, 2003) and resistance to alteration or replacement by reaction, these substitutions render zircon a premier geochronometer. Similarly, very low diffusion rates of trace elements and oxygen isotopes (Cherniak et al., 1997) allow retention of initial compositions and thereby can provide a record of conditions experienced during zircon growth. Of particular interest to economic geology is the utility of Ce and Eu anomalies in zircon as proxies for oxidation state, for which several studies have proposed a correlation between zircon Eu and Ce anomalies and Cu content in some ore-bearing rocks (e.g., Ballard et al., 2002; Liang et al., 2006; Dilles et al., 2015).

The Yerington copper mine in Yerington, Nevada, is an ideal location to study processes controlling formation of porphyry copper deposits. The geology of the Jurassic Yerington batholith and the copper-rich mineral deposits of the Yerington district are well studied (e.g., Proffett, 1979; Proffett and Dilles, 1984; Carten, 1986; Dilles, 1987; Dilles and Wright, 1988). The porphyry system exposed in the Yerington mine consists of three magmatic units, the youngest of which hosts several Cu-rich porphyry dikes (Fig. 1). Previous U-Pb thermal ionization mass spectrometry (TIMS) zircon ages (bulk separates) from plutonic and volcanic units from the Singatse and Buckskin Ranges, west of the Yerington mine, and showed that the ore-bearing porphyry dikes were emplaced between 169.4 and 168.5 Ma (Dilles and Wright, 1988). The study by Dilles and Wright (1988) focused on major igneous units associated with the Yerington batholith but did not extensively sample the Yerington mine porphyry dikes, and no microanalytical zircon ages from these units have previously been reported.

This study integrates new zircon U-Pb analyses with zircon trace element geochemistry and oxygen isotope compositions measured by secondary ion mass spectrometry (SIMS) to investigate (1) if there is any evidence of magma

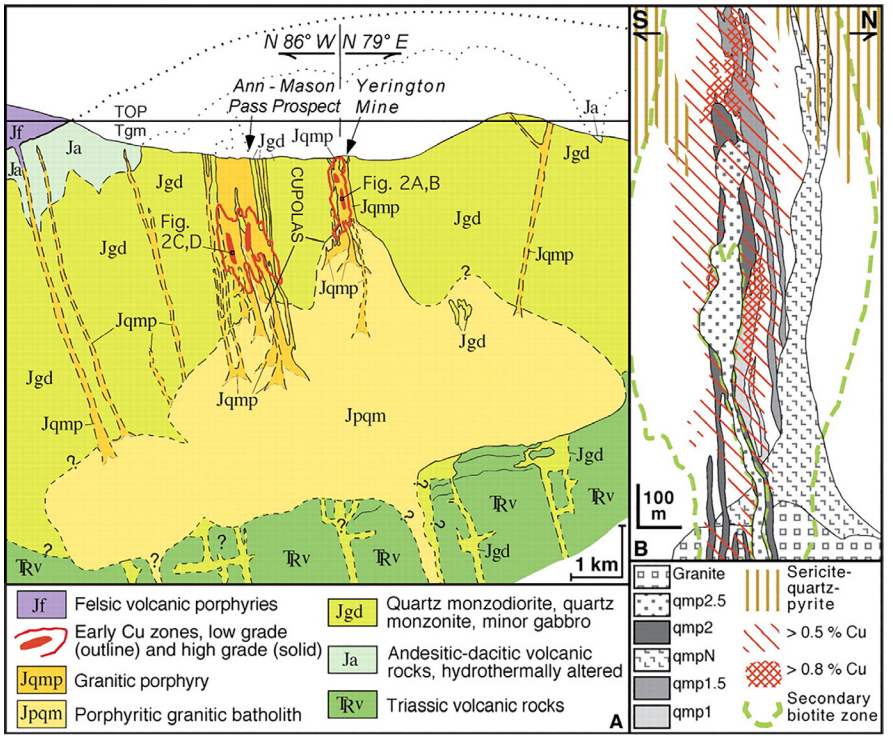


**Figure 1. (A) Pre-tilt paleogeologic cross section through Yerington district, Nevada, showing Mesozoic geology based on detailed geologic mapping (Proffett and Dilles, 1984). (B) Pre-tilt section through Yerington Mine from boxed area in (A). Legend lists porphyries by age, oldest at bottom, based on crosscutting relationships. Luhr Hill granite (Jpqm in A) is magmatic source of porphyries and fluids. From Proffett (2009). Unit names: Jqmp—porphyry dike; Jgd—McLeod Hill quartz monzodiorite; Jpqm—Luhr Hill granite. See Supplemental Tables (footnote 1) for equivalent unit nomenclature used in text.**

residence time or recycling suggested by spot analyses of zircon interiors that might reveal a longer history than resolved by multigrain TIMS bulk analysis (cf. Dilles and Wright, 1988); (2) controls on magmatic processes in Yerington mine ore-bearing units as recorded by zircon trace element chemistry (cf. Dilles et al., 2015) and oxygen isotope compositions; and (3) if thermal annealing and chemical abrasion (TA/CA) treatment of zircons that range from 90 to 2200 ppm U prior to sensitive high-resolution ion microprobe–reverse geometry (SHRIMP-RG) analysis improves the accuracy and precision of U-Pb age populations or affects trace element and oxygen isotope compositions. In addition, we consider the efficacy of laser Raman spectroscopy to pre-select analytical spots that avoid metamict zones.

## BACKGROUND AND MOTIVATION

### Geologic Background

The Yerington batholith was emplaced during Jurassic arc magmatism and subsequently faulted and rotated up to 90° during Cenozoic extension (Proffett, 1977), exposing a rough cross section through the magmatic porphyry copper system and associated hydrothermal regime (Fig. 1). Three units constitute the Yerington batholith. In order of decreasing age, these are: the McLeod Hill quartz monzodiorite (abbreviated in this paper as Jqmd, following Carten [1986] and Dilles [1987]; see Table S1 in Supplemental Tables[1] for summary of previously published unit nomenclature for Yerington units); the Bear quartz monzonite (Jbqm); and the Luhr Hill granite (Jpg), which hosts a series of copper ore-bearing porphyry dikes (Jgp) exposed in the Yerington mine (Dilles and Wright, 1988). The McLeod Hill quartz monzodiorite constitutes ~80% of the volume of the Yerington batholith (Dilles, 1987); zircon U-Pb TIMS geochronology indicates crystallization at 169.4 ± 0.4 Ma (Dilles and Wright, 1988). Dilles and Wright (1988) also reported a U-Pb zircon age of 168.5 ± 0.3 Ma for one of the Luhr Hill–derived porphyry dikes from the Ann-Mason area, ~2–3 km west of the Yerington mine. The porphyry dikes emanated from the top of the cupola-like Luhr Hill granite, aided by fluid overpressure or tectonic fracturing; the dikes were accompanied by magmatic-hydrothermal fluids that ultimately deposited economically viable amounts of bornite and chalcopyrite into and around the individual dike units (Fig. 1; Dilles et al., 2000; Proffett, 2009). Exposed within the Yerington mine are at least six granite porphyries, designated Jpg1, N (North; discovered after numerical sequence implemented), 1.5, 2, 2.5,

Table S1. Summary of Yerington unit nomenclature

| USGS classification[1] | Abbreviation (used in text) | Anaconda Company classification[2] | Analysis abbreviation in data tables |
|---|---|---|---|
| McLeod Hill quartz monzodiorite | Jgmd | Granodiorite | Jgd |
| Bear quartz monzonite | Jbqm | Bear quartz monzonite | Jbqm |
| Luhr Hill granite (porphyritic) | Jpg | porphyritic quartz monzonite | Jpqm |
| Luhr Hill granite porphyry dikes | Jpg(1, 1.5, 2, 3) | quartz monzonite porphyry | Jpmp (-1, -1.5, -2, -3) |

[1]Carten, 1986; Dilles, 1987; Dilles and Wright, 1988; Dilles et al., 2015; and others
[2]Proffett and Dilles, 1984; Proffett, 2009; former Anaconda Co. documents

[1]Supplemental Tables. Table S1 is a summary of Yerington unit nomenclature; Table S2 is a description of Yerington mine rocks; Table S3 contains laser Raman analyses and characterization; Table S4 contains in situ U-Pb zircon geochronology results; and Table S5 contains in situ zircon oxygen isotope compositions. Please visit http://doi.org/10.1130/GES01351.S1 or the full-text article on www.gsapubs.org to view the Supplemental Tables.

and 3, that decrease in age and Cu-ore content with increasing designation (i.e., Jgp1 is the oldest and most mineralized dike, while Jgp 3 is the youngest and least mineralized) (Proffett, 1979; Carten, 1986; Dilles et al., 2000; Proffett, 2009). It should be noted that the relative ages of the Jgp1 and JgpN dikes are uncertain, while the designation of Jgp1.5 as a separate unit is debated (Carten, 1986). This study assumes the existence of Jgp1.5 as a separate unit.

Mineralogy of the McLeod Hill quartz monzodiorite includes less than 20 vol% quartz (mostly in the groundmass), ~5%–10% hornblende, ~5% biotite, 50% plagioclase, 15%–20% potassium feldspar, and trace amounts of zircon, apatite, sphene, and Fe-Ti oxides in the groundmass (e.g., Carten, 1986; Dilles, 1987). The McLeod Hill quartz monzodiorite is relatively fine grained and equigranular. The Bear quartz monzonite is equigranular and ranges from fine grained (within several hundred meters of its outer borders) to medium grained in the interior of the unit. Mineralogy of the Bear unit includes biotite and hornblende (5–10 vol%), 45%–50% plagioclase, ~25% potassium feldspar, and ~20% quartz, with trace amounts of sphene, zircon, apatite, and Fe-Ti oxides. The Luhr Hill granite has a medium-grained, seriate to porphyritic texture and is characterized by ~10 vol% hornblende + biotite, ~40% plagioclase, 30% potassium feldspar (~5 vol% as 10 mm phenocrysts), 30% quartz, and trace zircon and sphene. All porphyry dike units have a similar texture: ~50% abundant 1–4 mm subhedral plagioclase, less abundant >1 cm potassium feldspar phenocrysts, sparse anhedral quartz, 5%–10% hornblende (often altered to biotite) and subhedral to euhedral biotite books, and trace sphene and ~50% aplitic (0.02–0.05 mm) groundmass of quartz and potassium feldspar (quartz < potassium feldspar) with trace biotite and plagioclase (Dilles, 1987). Jgp1 is >15% quartz veins; quartz vein density decreases with decreasing age of porphyry; Jgp3 is devoid of quartz veins. The porphyry dike units grade downward into the Luhr Hill granite via an increase in groundmass grain size (Dilles et al., 2000). All porphyry dike units exhibit varying degrees of alteration, with stronger secondary mineralization in the early porphyry dike units (Jgp1, N, and 1.5) linked to early potassic alteration. Sericitic alteration overprints all Yerington porphyry units, although the youngest porphyry (Jgp3) is less altered (Proffett, 2009). For a comprehensive summary of porphyry dikes and wall-rock physical characteristics, see Proffett and Dilles (1984); Carten (1986); Dilles (1987); and Dilles et al. (2000).

## Ce and Eu Anomalies in Zircon as Proxies for Oxidation States in Magmas

Ce and Eu both occur naturally in two valence states: Ce as $Ce^{3+}$ and $Ce^{4+}$, Eu as $Eu^{3+}$ and $Eu^{2+}$. This leads to natural fractionation of each pair of ions, and to anomalies in rare earth element (REE) patterns. $Ce^{3+}$ is the dominant species in magmas and is highly incompatible in zircon, but $Ce^{4+}$ has an ionic radius very similar to $Zr^{4+}$ and readily substitutes for it in zircon (Colombini et al., 2011). This results in elevated $Ce^{4+}/Ce^{3+}$ and the almost universal presence of a pronounced positive Ce anomaly ($Ce_N/Ce_N^*$, where $Ce_N^*$ is Ce concentration calculated from a log-linear chondrite-normalized REE pattern $\left[Ce_N^* = e^{\left(\ln(Nd_N)-\left(\ln(Sm_N)-\ln(Nd_N)\right)\right)}\right]$ in zircon. Because $Ce^{4+}$ constitutes such a small fraction of total Ce and no other mineral has such a strong relative affinity for it, melts and unaltered whole rocks have $Ce_N/Ce_N^*$ very near unity (e.g.,Trail et al., 2012). Oxygen fugacity of the parent magma and temperature of crystallization are thus the main controls on the $Ce^{4+}/Ce^{3+}$ ratio in zircon, and there is a direct relationship between $Ce^{4+}/Ce^{3+}$ and $Ce_N/Ce_N^*$ (e.g., Ballard et al., 2002; Trail et al., 2012). Conversely, $Eu^{2+}$ is more incompatible in zircon than $Eu^{3+}$, which leads to a negative Eu anomaly $\left(Eu_N/Eu_N^*, \text{where } Eu_N^* = e^{\left(\frac{\ln(Gd_N)-\ln(Sm_N)}{2}\right)-\ln(Sm_N)}\right)$ in zircon crystals compared with the melts from which they have grown.

Application of Ce and Eu anomalies to quantitatively unraveling magmatic conditions is not straightforward. Accurate calculation of the Ce anomaly ($Ce_N/Ce_N^*$) or the $Ce^{4+}/Ce^{3+}$ ratio in zircon is notoriously problematic (e.g., Ballard et al., 2002; Dilles et al., 2015; Trail et al., 2015, and references therein) due to extremely low concentrations of La, Pr, and Nd in zircon that may be artificially elevated by incorporation in analytical volumes of nanometer-scale inclusions of melt, apatite, monazite, allanite, chevkinite, and other minerals with high partition coefficients for light rare earth elements (LREEs). Calculation of $Ce_N/Ce_N^*$ by projecting back from more abundant Sm and Nd is more reliable than calculating from La and Pr (Ballard et al., 2002) but also requires assuming log-linear REE pattern from Sm through La. The method of $Ce^{4+}/Ce^{3+}$ determination used by Ballard et al. (2002) depends on the assumption that whole rock Ce content is equal to silicate liquid Ce content, which is not likely the case after substantial crystallization (Dilles et al., 2015). Recently, Trail et al. (2012) derived an experimentally based relationship between $Ce_N/Ce_N^*$ and oxygen fugacity, but this model tends to yield anomalous results that have questionable application for real magmatic systems (e.g., Wang et al., 2014; Dilles et al., 2015) and was subsequently downplayed by Trail et al. (2015).

Despite these issues, several studies have applied zircon Eu and Ce anomalies to qualitatively investigate variation in oxygen fugacity and oxidation of magmatic systems (Ballard et al., 2002; Burnham and Berry, 2012; Trail et al., 2012; Chelle-Michou et al., 2014; Dilles et al., 2015). Quantifying the oxidation and evolution of magmatic systems using zircon that crystallized within porphyry copper systems has the potential to provide constraints on the conditions of the magma system as it evolved prior to emplacement and/or eruption. This is important because copper in magma with high oxygen fugacity should become enriched during differentiation and is expected to partition into a magmatic-hydrothermal fluid (e.g., Dilles, 1987; Cline and Bodnar, 1991; Pasteris, 1996; Streck and Dilles, 1999Ulrich et al., 1999; Ballard et al., 2002; Sun et al., 2004). Increasing oxidation during system development is a hallmark of porphyry Cu systems (e.g., Dilles et al., 2000, 2015; and many others). As proof of concept, Ballard et al. (2002) and Dilles et al. (2015) found that zircon $Eu_N/Eu_N^*$>0.4 is characteristic of many porphyry copper ore-forming intrusions (Fig. 2). Similarly, Liang et al. (2006) show that Ce anomalies are significantly lower in zircons from barren rocks than ore-bearing rocks in the same system. Based on the available data for zircon Eu and Ce anomalies from the Yerington

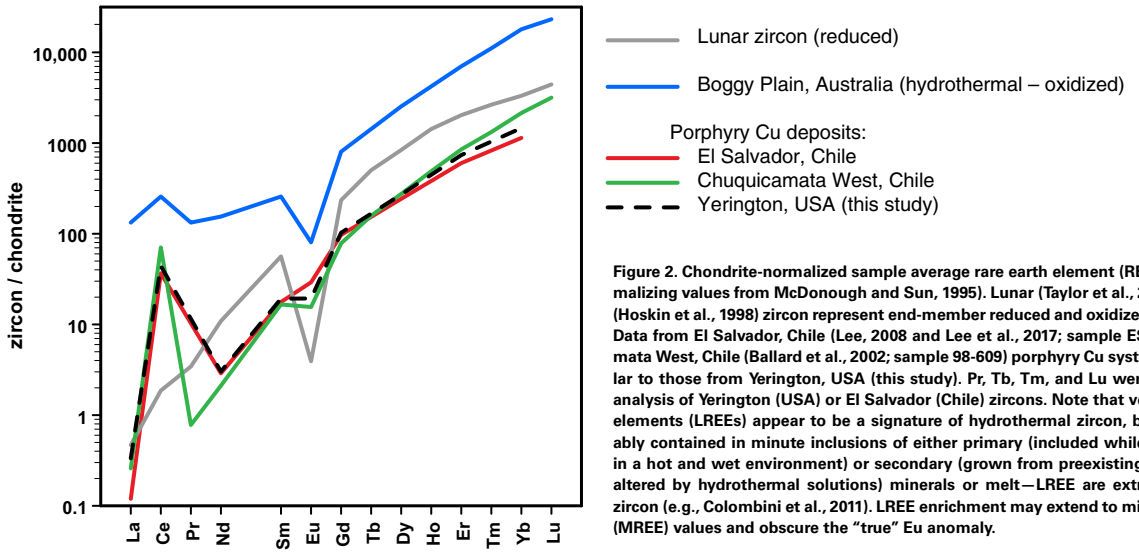


**Figure 2. Chondrite-normalized sample average rare earth element (REE) zircon patterns (normalizing values from McDonough and Sun, 1995). Lunar (Taylor et al., 2009) and hydrothermal (Hoskin et al., 1998) zircon represent end-member reduced and oxidized systems, respectively. Data from El Salvador, Chile (Lee, 2008 and Lee et al., 2017; sample ES-12807) and Chuquicamata West, Chile (Ballard et al., 2002; sample 98-609) porphyry Cu system zircon are very similar to those from Yerington, USA (this study). Pr, Tb, Tm, and Lu were not measured during analysis of Yerington (USA) or El Salvador (Chile) zircons. Note that very high light rare earth elements (LREEs) appear to be a signature of hydrothermal zircon, but the LREEs are probably contained in minute inclusions of either primary (included while zircons were growing in a hot and wet environment) or secondary (grown from preexisting zircon as it was being altered by hydrothermal solutions) minerals or melt—LREE are extremely incompatible in zircon (e.g., Colombini et al., 2011). LREE enrichment may extend to middle rare earth element (MREE) values and obscure the "true" Eu anomaly.**

intrusions and ore magmas, as well as other igneous rocks associated with porphyry mineral deposits (Dilles et al., 2015), we expect Yerington zircon Eu and Ce anomalies to reflect oxidizing conditions commensurate with the amount of mineralization in the ore-bearing rocks.

## TA/CA Treatment Prior to Zircon Geochronology via SHRIMP-RG

Zircon readily incorporates significant quantities of U into its crystal structure ($Kd_U^{zrc/melt} \approx 16–148$; Colombini et al., 2011), whereas Pb is excluded during crystallization due to lack of an appropriate structural site, which makes it an excellent mineral for U-Pb geochronology. However, the presence of radioactive elements (U and Th) in zircon poses potential problems due to radiation damage accumulated through time, resulting in an increasing number of crystal lattice defects and can ultimately produce a metamict state in zircon in which ionic diffusivities increase, including Pb mobility or loss, and isotope ratios and trace element concentrations may be affected (e.g., Wang et al., 2014 and references therein).

Removal of metamict or structurally damaged portions of zircon grains via thermal annealing and chemical abrasion (TA/CA) prior to analysis has been routine procedure for high-precision isotope dilution–thermal ionization mass spectrometry (ID-TIMS) U-Pb geochronology for over a decade (Mattinson, 2005). Chemical abrasion preferentially attacks portions of zircon that have highly damaged crystal structures and are amorphous. Because microanalytical methods require comparison of unknown grains to a standard material with similar composition and crystal structure (e.g., White and Ireland, 2012), analyzing partially or fully metamict zircons results in inaccurate data and commonly high analytical errors (e.g., Wang et al., 2014). Although common for TIMS, the TA/CA treatment has been applied to relatively few microanalytical U-Pb studies (e.g., laser ablation–inductively coupled plasma mass spectrometry [LA-ICPMS] or SIMS). Kryza et al. (2012) report results showing the TA/CA treated zircon population from a Carboniferous sample analyzed by SHRIMP-II that yielded ~5% older ages that were more reproducible than untreated grains from the same sample. They attribute older ages and improved reproducibility to removal of metamict zones susceptible to Pb loss from the TA/CA treated samples. A similar result for TA/CA treated zircon from Paleogene samples was observed by Watts et al. (2016). von Quadt et al. (2014) found that TA/CA treated zircons analyzed via LA-ICPMS yield more reproducible and yielded ~4%–6% older ages than non-treated grains. Lidzbarski (2014) attributed statistically significant age differences between TA/CA treated and non-treated zircons (100–500 ppm U; ca. 18–22 Ma) from the Peach Spring Tuff to Pb loss. Since the Yerington zircons are older than the Peach Spring Tuff, have similar U content, and are associated with fluids and mineralization, they could have similarly been affected by Pb loss. Although TA/CA treatment of zircons is intended to improve precision and reproducibility of U-Pb dates, no studies have heretofore reported an analysis of the effects of TA/CA treatment on $\delta^{18}O$ in zircon, and investigations of effects on trace element compositions are limited (cf. Watts et al., 2016). Over the past decade, U-Pb zircon dates have been combined with multiple types of compositional microanalytical techniques (i.e., trace elements, O isotopes, Hf isotopes, etc.) that are often performed

on the same grains. The greatest strength of microanalytical methods is high spatial resolution and the ability to target micron-scale variations in individual mineral grains. Thus, establishing the effect, if any, that TA/CA treatment has on the measured U-Pb-Th age, trace element or oxygen isotope composition is critical to evaluating the overall usefulness of TA/CA treatment of zircon.

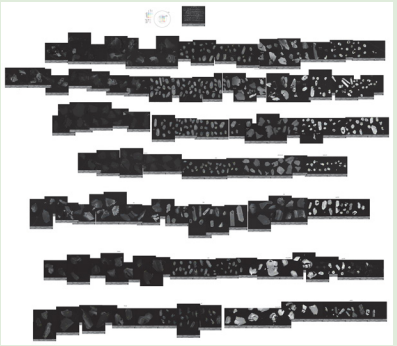

[2]Supplemental Plate contains cathodoluminescence images of Yerington zircons and corresponding analytical spots. Please visit http://doi.org/10.1130/GES01351.S2 or the full-text article on www.gsapubs.org to view the Supplemental Plate.

## METHODS

We collected four samples from ore-bearing Yerington porphyry dikes (units Jgp1, 1.5, 2, and 3) and three plutonic host units (Jbqm, Jpg, and Jqmd) from historic drill core intervals (Table 1). Historical and modern drill logs and assay data provided guidance while sampling and were used in the calculation of overall sample Cu grade. Thin sections of each sample were characterized at Vanderbilt University (VU) via petrographic microscope and a Tescan Vega 3 LM scanning electron microscope (SEM) with energy dispersive spectrometry (EDS) capabilities. Those observations are provided in the Supplemental Plate[2]. Zircon was extracted from the samples using standard crushing, sieving, and density separation techniques, followed by hand picking.

TABLE 1. SUMMARY OF YERINGTON MINE SAMPLES FROM HISTORIC CORE

| Sample | Drill hole | Depth (ft) | Description | Cu (%) |
|---|---|---|---|---|
| Jgp1 | L+100-16 | 65.5 | 1 piece, ~5 cm | 0.67 |
| | | 68 | 1 piece, ~7 cm | 0.67 |
| | | 69.4 | 1 piece, ~7 cm | 1.38 |
| | | 70 | 1 piece, ~7 cm | 1.38 |
| | M+16/M-16 | 41–41.7 | ~20 cm rubble | 0.58 |
| | | 49–49.8 | ~22 cm rubble | 0.57 |
| Jgp1.5 | Q+100-24 | 176.5–178 | ~45 cm rubble | 0.35 |
| | | 188 | 1 piece, ~9 cm | 0.35 |
| | | 189 | 1 piece, ~5 cm | 0.09 |
| Jgp2 | L+100-16 | 48 | 1 piece, ~6 cm | 0.37 |
| | | 53 | 1 piece, ~12 cm | 0.81 |
| | | 55.5 | 1 piece, ~10 cm | 0.81 |
| | | 57 | 1 piece, ~10 cm | 0.66 |
| Jgp3 | P+100-25 | 88 | 1 piece, ~7 cm | 0.06 |
| | | 98 | 1 piece, ~15 cm | 0.06 |
| | | 101 | 1 piece, ~15 cm | 0.06 |
| Jbqm | K+100-13 | 136–139 | ~90 cm rubble | 1.24 |
| Jpg | A+100-5S | 246 | 1 piece, ~9 cm | 0.09 |
| | | 251 | 1 piece, ~15 cm | 0.06 |
| | | 254.5 | 2 pieces, 7 cm | 0.07 |
| Jqmd | O-18 | 214–214 | ~60 cm rubble | 0.14 |
| | | 222 | 1 piece, ~11 cm | 0.16 |
| | | 224–226 | ~60 cm rubble | 0.14 |

About half the zircon from each sample underwent thermal annealing and chemical abrasion at Berkeley Geochronology Center following a procedure similar to that of Mundil et al. (2004). Crystals were annealed at 850 °C in uncovered quartz crucibles for 46 h, then rinsed in ethanol (EtOH), and transferred via pipette to Teflon microcapsules. Once the EtOH evaporated, capsules received 25 µL each of concentrated $HNO_3$ and HF and were placed inside pressurized bombs with 30 mL concentrated HF for 10 h at 220 °C. After cooling, each capsule received 25 µL concentrated $HNO_3$ and was placed on a hot plate for 2 h to re-suspend any precipitate. The liquid portion was decanted, and the treated zircons were rinsed in 100 µL EtOH and dried before mounting.

Thermal annealing and chemical abrasion (TA/CA) treated and untreated zircon grains from each sample, along with treated and untreated zircon standards Temora-2 and Mount Dromedary and untreated R33 and MADDER (in-house compositional standard at Stanford–U.S. Geological Survey [USGS] SHRIMP-RG laboratory; Barth and Wooden, 2010), were mounted in a single epoxy mount and polished to roughly midsection.

### Laser Raman Spectroscopy

Laser Raman spectroscopy analyses were performed on polished and imaged zircons at the Stanford University Extreme Environments Laboratory using a Renishaw inVIA confocal laser microRaman spectrometer equipped with a charge-coupled device (CCD). Measurements were conducted at 23 °C with 10 mW operating power and 514 nm light from the $Ar^+$ laser with a ~5 µm spot diameter. The spectral frequency resolution of the Raman spectrometer was 1–2 $cm^{-1}$, and the measurement range was 100–1500 $cm^{-1}$ using a static scan centered at 520 $cm^{-1}$, acquisition time of 5 s, and grating of 1800 grooves/mm. Spectra were collected using WIRE2 software. Amplitudes (Raman intensities) and detected full width half maximum (FWHM) for different peaks were obtained using OriginLab software (v. 9.0). Spectral peaks were detected if greater than 10% difference from background. FWHM corrections were applied using the approach of Irmer (1985) and Wang et al. (2014). We focused on bands $B_{1g}$ ($\nu_3$ [$SiO_4$]), $A_{1g}$ ($\nu_2$ [$SiO_4$]), and $E_g$ (I [Si-Zr]), which have peaks at ~1005 $cm^{-1}$, ~435 $cm^{-1}$, and ~355 $cm^{-1}$, respectively, in zircon (Dawson et al., 1971; Syme et al., 1977; Nasdala et al., 1998; Wang et al., 2014). Complete laser Raman spectral analysis results are in the Supplemental Tables (see footnote 1).

### SHRIMP-RG Analysis: U-Pb and Trace Elements

After laser Raman analysis, the epoxy mount was cleaned and gold-coated. Zircon U-Pb dating combined with trace element analysis (Ti, Fe, Y, REE, U, and Th) were performed on the Stanford–USGS SHRIMP-RG at Stanford University using an $O_2^-$ beam focused to a ~25 × 25 µm analytical spot. The complete U-Pb data set is given in Table S4 (see footnote 1). Analyses of Temora-2 zircon standard ($^{206}Pb/^{238}U$ age = 416.8 Ma; Black et al., 2004), both treated and

untreated, were performed after every four unknown analyses. Treated and untreated grains of Mount Dromedary zircon ($^{206}Pb/^{238}U$ age = 99.12 Ma; Schoene et al., 2006) were analyzed as a secondary standard interspersed within unknown analyses. Trace element concentrations were standardized using MADDER (3435 ppm U; Barth and Wooden, 2010). Data were reduced using Squid 2.51 (Ludwig, 2009) and Isoplot 3.76 software (Ludwig, 2012). The measured $^{206}Pb/^{238}U$ was corrected for common $Pb_c$ using $^{207}Pb$ using measured $^{207}Pb/^{206}Pb$ (Ireland and Williams, 2003) and a model Pb composition from Stacey and Kramers (1975). Weighted-mean age (2σ SE) results are summarized in Table 2 and Supplemental Table S4 (see footnote 1).

### CAMECA ims1270 Analysis: Oxygen Isotopes

Zircons were re-imaged on the VU SEM after SHRIMP-RG analysis, and the mount was lightly polished to remove existing analytical spots. After cleaning and gold-coating, oxygen isotope ratios were measured on the CAMECA ims1270 microprobe at University of California, Los Angeles (UCLA). Operating conditions include a $Cs^+$ beam ~25 × 15 μm and sputter depth of ~1 μm. Instrumental mass fractionation was determined using analyses of R33 standard zircons (5.55‰; Black et al., 2004). One-sigma external reproducibility in R33 was 0.33‰. Data reduction was performed with *Isotope*® software. Oxygen data are reported as $\delta^{18}O$‰ values with 2σ total error, calculated relative to Vienna standard mean ocean water (VSMOW; Baertschi, 1976). Backscatter electron (BSE) and secondary electron (SE) images were obtained using the VU Tescan Vega 3 LM SEM after analysis to inspect analytical pit locations. Thirty-four out of a total of 124 analyses that intersected significant cracks or inclusions or were partially off the grain were discarded. Results are listed in Table 2, and the complete data set is available in Table S5 (see footnote 1).

## RESULTS

### Laser Raman Spectroscopy

In total, 118 TA/CA treated and untreated zircon grains were analyzed by laser Raman that also underwent U-Pb age, trace element, and $\delta^{18}O$ analysis. Of those 118, 29 grains (27 Yerington zircons and two Mount Dromedary standard zircons) were specifically chosen for SIMS U-Pb and trace element analysis because the Raman spectra had lower FWHM and/or additional peaks compared to the main three peaks (~1005 $cm^{-1}$, ~435 $cm^{-1}$, and ~355 $cm^{-1}$) of ideal crystalline zircon (e.g., Fig. 3) that indicated unannealed radiation damage or a potentially metamict area in the grain (cf. Zhang et al., 2000). We identified 13 additional peaks that were >10% above the baseline; the most prominent occurred at ~224 $cm^{-1}$ (16.1% of grains), ~973 $cm^{-1}$ (12.7%), ~1462 $cm^{-1}$ (6.5%), ~201 $cm^{-1}$ (4.2%), ~1111 $cm^{-1}$ (3.4%), and <2.5% of grains at ~121, 129, 222, 1054, 1087, 1143, 1457, and 1611 $cm^{-1}$. Peaks at ~224 and 973 $cm^{-1}$, which account for 52% of the extra peaks recorded, are characteristic of crystalline zircon (Dawson et al., 1971; Syme et al., 1977; Zhang et al., 2000), though they are not the primary crystalline zircon peaks (~1005 $cm^{-1}$, ~435 $cm^{-1}$, and ~355 $cm^{-1}$). Of the 29 grains with extra Raman peaks, only six have three or more peaks present.

Of the 29 grains with Raman spectra that displayed additional peaks, only one had an anomalously young (163 ± 2 Ma) U-Pb age result (Jpqmcata_3.1), and five grains yielded anomalously low $\delta^{18}O$ results (see Supplemental Table S5 [footnote 1]). Trace element data for four of the six grains with ≥3 laser Raman peaks contained higher trace element concentrations when compared to both treated and untreated grains from the same sample. Trace element concentrations in grains with two or fewer additional peaks did not vary systematically from trace element concentrations in treated and untreated grains with no additional peaks from the same sample.

### U-Pb Zircon Geochronology

$^{207}Pb_c$-corrected $^{206}Pb/^{238}U$ ages of Yerington zircons are Jurassic, ranging from 162 ± 3 Ma to 174 ± 3 Ma (individual grains, 1σ error), which agrees with previous TIMS ages of Dilles and Wright (1988). There is no statistically significant difference between weighted-mean sample ages from grains that underwent TA/CA treatment and untreated grains from the same sample (Tables 2 and 3; Fig. 4). Non-porphyry units (Jqmd, Jbqm, and Jpg) have statistically identical weighted-mean ages (including treated and untreated grains) of 170.0 ± 1.4 Ma [n = 7; mean square of weighted deviates (MSWD) = 1.44]; 169.6 ± 1.3 Ma [n = 14; MSWD = 1.35]; and 169.4 ± 1.5 Ma [n = 8; MSWD = 0.61], respectively. All errors are 2 SE. Weighted-mean ages of porphyry dike units (Jgp1: 169.0 ± 1.2 Ma [n = 20; MSWD = 1.50]; Jgp1.5: 168.7 ± 1.1 Ma [n = 20; MSWD = 1.58]; and Jgp2: 168.7 ± 1.2 Ma [n = 16; MSWD = 1.63]) are also statistically identical. It should be noted that these age results for Jqmd and the porphyry dikes are within error of those obtained via TIMS by Dilles and Wright (1988) but are less precise.

Treated and untreated secondary standards Mount Dromedary and Temora-2 vary in calculated age and reproducibility. Treated Mount Dromedary grains have a weighted-mean age of 100.0 ± 1.7 Ma (n = 4; MSWD = 0.08), while untreated Mount Dromedary yields a weighted- mean age of 98.4 ± 4.9 Ma (n = 4; MSWD = 5.22). Both are within uncertainty of each other and the published TIMS age of 99.12 ± 0.14 Ma (Schoene et al., 2006), but the untreated grains are less reproducible, although this observation is based on a limited number of analyses. Mount Dromedary ages calculated using untreated Temora-2 as the age primary standard also agree with the published age of 98.8 ± 0.6 reported by White and Ireland (2012) at the 2σ level. Combined, the weighted-mean age of Mount Dromedary treated and untreated zircon is 99.1 ± 2.0 Ma (n = 8; MSWD = 2.61). Temora-2 untreated and treated grains have a combined weighted-mean age of 419.0 ± 1.6 Ma (n = 35; MSWD = 1.3) when referenced to Mount Dromedary ages, which is older than the published age of 416.8 Ma ± 0.33 (Black et al., 2004).

TABLE 2. SUMMARY OF YERINGTON ZIRCON ANALYTICAL RESULTS

| | Laser Raman | | Age | | | | | | | | | | | | | | | | | | | | Oxygen | |
|---|---|---|---|---|---|---|---|---|---|---|---|---|---|---|---|---|---|---|---|---|---|---|---|---|
| Analysis | Amplitude (counts) | FWHM ($cm^{-1}$) | $^{206}Pb/^{238}U$ (Ma) | 1σ | Th (ppm) | U (ppm) | Y (ppm) | La (ppm) | Ce (ppm) | Nd (ppm) | Sm (ppm) | Eu (ppm) | Gd (ppm) | Dy (ppm) | Er (ppm) | Yb (ppm) | Hf (ppm) | $Eu_N/Eu_N^*$ | $Ce_N/Ce_N^*$ | Ti (ppm) | Fe (ppm) | T (°C) | $\delta^{18}O$ (‰) | 2σ total |
| Jgp1 | | | | | | | | | | | | | | | | | | | | | | | | |
| qmp1_1.1 | 34207 | 6.4 | 168 | 4 | 90 | 179 | 350 | 0.01 | 22.62 | 0.27 | 1.13 | 0.43 | 8.7 | 31.8 | 63.1 | 126 | 10682 | 0.41 | 812 | 7.4 | 0.3 | 751 | | |
| qmp1_3.1 | 15761 | 6.6 | 165 | 3 | 98 | 199 | 338 | 0.01 | 17.22 | 0.65 | 1.18 | 0.65 | 8.2 | 28.7 | 60.5 | 145 | 9419 | 0.63 | 110 | 5.0 | 0.2 | 716 | 5.64 | 0.68 |
| qmp1_4.1 | 19002 | 6.5 | 168 | 2 | 174 | 299 | 380 | 0.01 | 22.38 | 0.71 | 1.23 | 0.63 | 9.1 | 31.1 | 68.3 | 177 | 9807 | 0.58 | 127 | 5.3 | 0.2 | 721 | | |
| qmp1_5.1 | 41566 | 5.9 | 170 | 3 | 98 | 142 | 504 | 0.02 | 17.95 | 0.88 | 2.16 | 0.68 | 15.0 | 51.2 | 86.1 | 167 | 10036 | 0.36 | 116 | 13.3 | 0.2 | 810 | 6.00 | 0.67 |
| qmp1_6.1 | 40292 | 5.7 | 169 | 2 | 93 | 149 | 480 | 0.01 | 17.73 | 0.73 | 2.09 | 0.67 | 15.5 | 48.1 | 83.0 | 160 | 10943 | 0.36 | 161 | 11.8 | 0.2 | 798 | 5.82 | 0.65 |
| qmp1_7 | | | | | | | | | | | | | | | | | | | | | | | 4.55 | 0.65 |
| qmp1_8 | | | | | | | | | | | | | | | | | | | | | | | 5.92 | 0.67 |
| qmp1_10.1 | 45261 | 6.7 | 173 | 2 | 631 | 863 | 589 | 0.02 | 48.34 | 0.79 | 2.02 | 1.02 | 15.4 | 51.4 | 103.9 | 237 | 10329 | 0.56 | 357 | 6.9 | 1.0 | 745 | | |
| qmp1_13.1 | 16284 | 6.5 | 171 | 1 | 303 | 475 | 411 | 0.20 | 26.88 | 0.54 | 0.99 | 0.59 | 8.3 | 32.1 | 69.5 | 175 | 9321 | 0.63 | 211 | 5.6 | 105.2 | 726 | | |
| qmp1_14.1 | 29273 | 6.2 | 168 | 2 | 147 | 190 | 649 | 0.02 | 18.97 | 1.56 | 2.85 | 0.89 | 21.8 | 67.3 | 111.4 | 212 | 9457 | 0.34 | 52 | 15.9 | 0.8 | 829 | 5.63 | 0.65 |
| qmp1_15.1 | 24160 | 5.8 | 168 | 2 | 291 | 315 | 925 | 0.05 | 28.28 | 2.93 | 5.53 | 1.67 | 35.2 | 100.7 | 153.0 | 274 | 9544 | 0.37 | 42 | 16.0 | 0.9 | 830 | 5.93 | 0.64 |
| qmp1_16 | | | | | | | | | | | | | | | | | | | | | | | 5.67 | 0.67 |
| qmp1_17 | | | | | | | | | | | | | | | | | | | | | | | 5.62 | 0.68 |
| qmp1_19.1 | 31547 | 5.9 | 167 | 8 | 95 | 157 | 369 | 0.07 | 15.55 | 0.47 | 1.16 | 0.47 | 9.6 | 34.2 | 64.3 | 138 | 10072 | 0.43 | 192 | 14.2 | 23.2 | 817 | 5.34 | 0.68 |
| qmp1_20 | | | | | | | | | | | | | | | | | | | | | | | 5.33 | 0.69 |
| qmp1_24 | | | | | | | | | | | | | | | | | | | | | | | 5.23 | 0.67 |
| qmp1_28 | | | | | | | | | | | | | | | | | | | | | | | 5.81 | 0.67 |
| qmp1_29 | | | | | | | | | | | | | | | | | | | | | | | 5.40 | 0.66 |
| qmp1_30 | | | | | | | | | | | | | | | | | | | | | | | 5.75 | 0.65 |
| Jgp1 (TA/CA) | | | | | | | | | | | | | | | | | | | | | | | | |
| qmp1cata_1.1 | 42003 | 5.5 | 166 | 3 | 120 | 216 | 406 | 0.05 | 20.73 | 0.53 | 1.27 | 0.61 | 11.2 | 38.6 | 70.8 | 145 | 8940 | 0.49 | 216 | 12.9 | 0.2 | 807 | | |
| qmp1cata_3.1 | 27353 | 5.9 | 170 | 2 | 129 | 284 | 280 | 0.01 | 19.31 | 0.36 | 0.67 | 0.35 | 5.4 | 21.7 | 49.5 | 130 | 10142 | 0.57 | 234 | 5.5 | 0.3 | 724 | 5.38 | 0.65 |
| qmp1cata_4.1 | 16361 | 6.3 | | | | | | | | | | | | | | | | | | | | | | |
| qmp1cata_5.1 | 27308 | 6.0 | | | | | | | | | | | | | | | | | | | | | | |
| qmp1cata_6.1 | 3082 | 19.1 | 169 | 3 | 1943 | 1197 | 2547 | 0.11 | 79.98 | 4.99 | 10.75 | 3.34 | 78.8 | 258.8 | 422.8 | 752 | 9360 | 0.35 | 80 | 19.7 | 0.5 | 853 | | |
| qmp1cata_7.1 | 31003 | 5.9 | | | 430 | 375 | 1207 | 1.92 | 52.95 | 4.40 | 8.53 | 2.72 | 51.4 | 126.9 | 191.9 | 322 | 5542 | 0.40 | 54 | 14.8 | 3.0 | 821 | | |
| qmp1cata_8.1 | 21080 | 5.7 | | | 285 | 384 | 937 | 0.27 | 43.10 | 2.27 | 4.65 | 1.80 | 30.6 | 92.9 | 152.6 | 305 | 10045 | 0.46 | 89 | 7.5 | 3.4 | 752 | | |
| qmp1cata_9.1 | 11281 | 5.7 | | | 95 | 158 | 558 | 0.01 | 18.27 | 1.22 | 2.60 | 0.99 | 17.3 | 54.8 | 95.3 | 191 | 9817 | 0.45 | 74 | 9.1 | 0.2 | 772 | | |
| qmp1cata_10.1 | 44515 | 5.5 | 170 | 4 | 121 | 224 | 352 | 1.58 | 41.03 | 1.26 | 1.38 | 0.45 | 8.8 | 30.1 | 58.4 | 124 | 10480 | 0.40 | 83 | 7.4 | 4.4 | 751 | | |
| qmp1cata_12.1 | 8974 | 5.6 | 167 | 3 | 138 | 168 | 676 | 0.02 | 21.81 | 2.01 | 3.88 | 1.13 | 23.8 | 69.6 | 112.5 | 205 | 9500 | 0.36 | 48 | 14.9 | 0.3 | 822 | | |
| qmp1cata_13.1 | 14971 | 8.0 | 170 | 4 | 965 | 974 | 3152 | 0.05 | 46.06 | 4.43 | 7.36 | 2.59 | 75.3 | 301.5 | 549.6 | 1006 | 9806 | 0.33 | 40 | 16.5 | 1.2 | 833 | 5.51 | 0.65 |
| qmp1cata_14.1 | 25244 | 6.0 | 169 | 6 | 46 | 94 | 281 | 0.04 | 12.61 | 0.34 | 1.01 | 0.40 | 6.9 | 25.8 | 49.0 | 103 | 10058 | 0.47 | 256 | 11.4 | 0.3 | 794 | 5.88 | 0.64 |
| Jgp1.5 | | | | | | | | | | | | | | | | | | | | | | | | |
| qmp1.5_1.1 | 36134 | 5.8 | 173 | 2 | 79 | 173 | 413 | 0.01 | 16.41 | 0.50 | 1.33 | 0.51 | 9.7 | 37.3 | 71.5 | 155 | 9762 | 0.43 | 200 | 11.8 | 0.2 | 798 | | |
| qmp1.5_2.1 | 49247 | 6.0 | 164 | 3 | 61 | 155 | 232 | 0.04 | 16.21 | 0.17 | 0.57 | 0.30 | 5.0 | 20.1 | 42.4 | 95 | 10969 | 0.54 | 714 | 5.4 | 0.2 | 722 | 6.00 | 0.68 |
| qmp1.5_3 | | | | | | | | | | | | | | | | | | | | | | | 4.97 | 0.65 |
| qmp1.5_4.2 | 46932 | 6.0 | 168 | 3 | 65 | 151 | 276 | 0.00 | 17.78 | 0.23 | 0.81 | 0.32 | 6.8 | 25.1 | 49.5 | 110 | 10470 | 0.42 | 650 | 7.6 | 0.3 | 754 | 5.78 | 0.66 |
| qmp1.5_5 | | | | | | | | | | | | | | | | | | | | | | | 4.84 | 0.65 |
| qmp1.5_6.1 | 25758 | 6.2 | 165 | 3 | 73 | 187 | 224 | 0.01 | 15.63 | 0.18 | 0.60 | 0.28 | 4.4 | 16.9 | 39.6 | 98 | 11140 | 0.53 | 644 | 5.0 | 0.3 | 716 | 5.74 | 0.66 |
| qmp1.5_8.1 | 49393 | 5.8 | 169 | 2 | 64 | 149 | 292 | 0.04 | 18.99 | 0.21 | 0.83 | 0.34 | 7.1 | 23.2 | 52.5 | 117 | 10829 | 0.42 | 816 | 6.5 | 0.4 | 739 | | |
| qmp1.5_9.1 | 41237 | 7.3 | 169 | 2 | 836 | 717 | 2333 | 0.11 | 79.67 | 6.84 | 14.26 | 6.08 | 91.3 | 258.1 | 378.4 | 645 | 8532 | 0.51 | 56 | 18.4 | 0.2 | 846 | | |
| qmp1.5_10.1 | 44848 | 5.8 | 167 | 3 | 110 | 220 | 285 | 0.02 | 14.33 | 0.88 | 1.24 | 0.62 | 8.1 | 25.1 | 51.8 | 125 | 10667 | 0.60 | 53 | 3.8 | 0.3 | 693 | 5.34 | 0.67 |
| qmp1.5_11 | | | | | | | | | | | | | | | | | | | | | | | 5.85 | 0.67 |
| qmp1.5_12 | | | | | | | | | | | | | | | | | | | | | | | 5.63 | 0.66 |
| qmp1.5_24.1 | 34869 | 5.8 | 172 | 2 | 150 | 326 | 469 | 0.01 | 25.52 | 0.44 | 1.15 | 0.54 | 9.8 | 39.5 | 82.3 | 193 | 10389 | 0.49 | 355 | 6.0 | 0.3 | 731 | 5.48 | 0.65 |
| qmp1.5_25.1 | 19082 | 6.3 | 167 | 1 | 263 | 397 | 530 | 0.03 | 27.54 | 1.42 | 2.70 | 1.21 | 15.8 | 48.4 | 91.4 | 206 | 10598 | 0.57 | 85 | 5.2 | 0.3 | 719 | | |
| qmp1.5_26.1 | 45383 | 5.8 | 165 | 3 | 145 | 305 | 441 | 0.01 | 31.46 | 0.49 | 1.30 | 0.55 | 9.9 | 36.3 | 78.3 | 182 | 10449 | 0.47 | 391 | 6.2 | 0.3 | 734 | 5.82 | 0.66 |
| qmp1.5_28 | | | | | | | | | | | | | | | | | | | | | | | 5.13 | 0.67 |

(*continued*)

TABLE 2. SUMMARY OF YERINGTON ZIRCON ANALYTICAL RESULTS (*continued*)

| | Laser Raman | | Age | | | | | | | | | | | | | | | | | | | Oxygen | |
|---|---|---|---|---|---|---|---|---|---|---|---|---|---|---|---|---|---|---|---|---|---|---|---|
| Analysis | Amplitude (counts) | FWHM ($cm^{-1}$) | $^{206}Pb/^{238}U$ (Ma) | 1σ | Th (ppm) | U (ppm) | Y (ppm) | La (ppm) | Ce (ppm) | Nd (ppm) | Sm (ppm) | Eu (ppm) | Gd (ppm) | Dy (ppm) | Er (ppm) | Yb (ppm) | Hf (ppm) | $Eu_N/Eu_N^*$ | $Ce_N/Ce_N^*$ | Ti (ppm) | Fe (ppm) | T (°C) | $\delta^{18}O$ (‰) | 2σ total |
| Jgp1.5 (TA/CA) | | | | | | | | | | | | | | | | | | | | | | | |
| qmp1.5cata_1.1 | | | | | | | | | | | | | | | | | | | | | | | 3.39 0.65 |
| qmp1.5cata_2.1 | 10426 | 5.8 | 170 | 2 | 103 | 225 | 268 | 0.01 | 19.98 | 0.30 | 0.81 | 0.27 | 6.8 | 24.1 | 48.7 | 102 | 11633 | 0.35 | 424 | 5.9 | 0.4 | 730 | | |
| qmp1.5cata_3.1 | 33145 | 5.7 | | | | | | | | | | | | | | | | | | | | | 4.82 0.67 |
| qmp1.5cata_3.2 | 46451 | 5.4 | 169 | 2 | 172 | 308 | 622 | 0.02 | 26.47 | 1.28 | 2.86 | 1.19 | 19.6 | 58.5 | 107.9 | 223 | 11243 | 0.48 | 106 | 4.8 | 0.3 | 711 | | |
| qmp1.5cata-4.1 | 21782 | 5.7 | 166 | 4 | 150 | 278 | 386 | 0.01 | 12.96 | 0.77 | 1.68 | 0.76 | 11.7 | 34.9 | 64.6 | 133 | 9781 | 0.52 | 85 | 5.3 | 0.4 | 720 | | |
| qmp1.5cata-5.1 | 47309 | 5.5 | 172 | 2 | 285 | 429 | 866 | 0.01 | 31.20 | 2.14 | 4.51 | 1.61 | 29.9 | 86.5 | 141.4 | 274 | 10175 | 0.42 | 71 | 6.3 | 0.2 | 736 | | |
| qmp1.5cata-6.1 | 66492 | 5.5 | 170 | 3 | 167 | 298 | 516 | 0.02 | 27.96 | 0.68 | 1.86 | 0.66 | 12.2 | 47.3 | 90.1 | 192 | 10245 | 0.42 | 262 | 10.6 | 0.4 | 787 | | |
| qmp1.5cata-7.1 | 31127 | 5.4 | 172 | 3 | 144 | 257 | 479 | 0.01 | 26.33 | 0.58 | 1.71 | 0.64 | 11.4 | 42.2 | 85.4 | 175 | 9608 | 0.44 | 309 | 10.8 | 0.2 | 788 | | |
| qmp1.5cata-8.1 | 19989 | 5.5 | 166 | 2 | 146 | 214 | 711 | 0.03 | 22.25 | 1.70 | 3.30 | 1.17 | 22.5 | 71.0 | 121.6 | 233 | 9992 | 0.41 | 58 | 9.6 | 0.3 | 776 | | |
| qmp1.5cata_10.1 | 20329 | 5.8 | 162 | 3 | 67 | 134 | 290 | 0.09 | 17.04 | 0.35 | 0.90 | 0.33 | 7.7 | 27.8 | 50.0 | 107 | 9364 | 0.39 | 285 | 9.3 | 1.3 | 773 | | |
| qmp1.5cata_12.1 | 40640 | 5.2 | 168 | 3 | 278 | 381 | 947 | 0.09 | 39.37 | 1.77 | 4.17 | 1.53 | 29.2 | 91.4 | 160.2 | 298 | 8633 | 0.42 | 120 | 7.8 | 0.8 | 757 | | |
| qmp1.5cata_15.1 | 21279 | 5.3 | 167 | 2 | 385 | 469 | 1193 | 0.06 | 48.53 | 2.29 | 5.00 | 2.01 | 39.6 | 115.8 | 196.4 | 355 | 9704 | 0.44 | 107 | 7.6 | 2.0 | 753 | | |
| Jgp2 | | | | | | | | | | | | | | | | | | | | | | | |
| qmp2_1.1 | 34630 | 6.0 | 164 | 2 | 106 | 244 | 221 | 0.02 | 14.93 | 0.24 | 0.53 | 0.31 | 4.6 | 16.6 | 39.1 | 103 | 10660 | 0.62 | 311 | 4.3 | 5.4 | 702 | | |
| qmp2_2.1 | 29639 | 6.0 | 171 | 2 | 204 | 344 | 312 | 0.04 | 23.19 | 0.64 | 0.89 | 0.86 | 6.9 | 26.1 | 56.8 | 127 | 10617 | 1.05 | 118 | 6.3 | 2.0 | 736 | | |
| qmp2_3.1 | 37981 | 5.5 | 170 | 2 | 49 | 131 | 158 | 0.00 | 12.35 | 0.14 | 0.46 | 0.20 | 3.6 | 12.4 | 27.9 | 67 | 11119 | 0.49 | 650 | 3.8 | 0.2 | 692 | | |
| qmp2_4.1 | 25154 | 6.0 | 173 | 4 | 86 | 179 | 224 | 0.01 | 10.45 | 0.42 | 0.97 | 0.50 | 6.3 | 18.7 | 37.6 | 94 | 10896 | 0.61 | 136 | 3.6 | 0.2 | 687 | | |
| qmp2_5.1 | 20884 | 5.7 | 172 | 5 | 269 | 421 | 328 | 0.01 | 28.63 | 0.48 | 0.90 | 0.61 | 7.0 | 24.6 | 58.7 | 152 | 10382 | 0.73 | 255 | 5.3 | 0.3 | 720 | 5.25 | 0.67 |
| qmp2_6.1 | 42429 | 6.1 | 170 | 1 | 252 | 398 | 653 | 0.02 | 22.77 | 2.17 | 3.39 | 1.74 | 21.4 | 61.7 | 109.3 | 241 | 10101 | 0.62 | 38 | 4.6 | 0.2 | 708 | 5.26 | 0.66 |
| qmp2_7.1 | 11732 | 6.3 | 164 | 3 | 137 | 290 | 311 | 0.07 | 19.58 | 0.47 | 0.82 | 0.47 | 6.0 | 25.7 | 57.0 | 149 | 10715 | 0.65 | 164 | 7.4 | 6.1 | 751 | 5.37 | 0.65 |
| qmp2_8.1 | | | | | | | | | | | | | | | | | | | | | | | 5.21 | 0.67 |
| qmp2_9.1 | 48734 | 5.6 | 168 | 1 | 247 | 408 | 667 | 0.02 | 28.18 | 1.29 | 2.64 | 1.17 | 18.9 | 64.6 | 115.6 | 236 | 10438 | 0.51 | 103 | 8.5 | 0.2 | 764 | | |
| qmp2_10.1 | | | | | | | | | | | | | | | | | | | | | | | 5.23 | 0.65 |
| qmp2_12 | | | | | | | | | | | | | | | | | | | | | | | 5.05 | 0.67 |
| qmp2_14 | | | | | | | | | | | | | | | | | | | | | | | 5.63 | 0.69 |
| qmp2_15 | | | | | | | | | | | | | | | | | | | | | | | 5.14 | 0.67 |
| qmp2_18 | | | | | | | | | | | | | | | | | | | | | | | 5.15 | 0.66 |
| qmp2_19 | | | | | | | | | | | | | | | | | | | | | | | 5.72 | 0.67 |
| Jgp2 (TA/CA) | | | | | | | | | | | | | | | | | | | | | | | |
| qmp2cata_1.1 | 29553 | 5.4 | 169 | 2 | 174 | 341 | 231 | 0.02 | 20.83 | 0.34 | 0.81 | 0.39 | 6.1 | 18.9 | 39.7 | 95 | 10292 | 0.53 | 338 | 4.6 | 0.3 | 709 | | |
| qmp2cata_2.1 | 59662 | 5.3 | 165 | 3 | 255 | 415 | 712 | 0.01 | 29.80 | 1.39 | 3.03 | 0.97 | 21.7 | 68.9 | 120.9 | 238 | 10560 | 0.37 | 107 | 10.5 | 0.2 | 785 | 4.06 | 0.67 |
| qmp2cata_3.1 | 12902 | 5.9 | 171 | 2 | 121 | 259 | 293 | 0.01 | 18.28 | 0.29 | 0.72 | 0.42 | 6.2 | 23.9 | 52.3 | 131 | 10413 | 0.61 | 365 | 4.8 | 0.2 | 712 | | |
| qmp2cata_4.1 | 46228 | 5.2 | 173 | 2 | 156 | 265 | 557 | 0.00 | 36.59 | 0.89 | 1.77 | 0.92 | 14.6 | 49.4 | 95.8 | 210 | 9634 | 0.55 | 190 | 6.2 | 0.2 | 735 | | |
| qmp2cata_5.1 | 41850 | 5.5 | 168 | 3 | 234 | 360 | 668 | 0.02 | 25.17 | 1.84 | 3.36 | 1.50 | 21.9 | 61.7 | 108.6 | 222 | 9695 | 0.53 | 57 | 4.9 | 0.2 | 713 | 4.20 | 0.66 |
| qmp2cata_6.1 | 42205 | 5.6 | 168 | 3 | 105 | 209 | 328 | 0.21 | 20.84 | 0.35 | 0.90 | 0.30 | 8.0 | 29.7 | 56.4 | 120 | 10117 | 0.34 | 345 | 10.1 | 0.4 | 781 | | |
| qmp2cata_8.1 | 36180 | 5.6 | 169 | 2 | 136 | 262 | 271 | 0.01 | 15.79 | 0.61 | 1.03 | 0.57 | 6.9 | 21.9 | 45.8 | 113 | 10320 | 0.65 | 101 | 4.5 | 0.3 | 707 | | |
| qmp2cata_9.1 | | | | | | | | | | | | | | | | | | | | | | | 4.75 | 0.65 |
| qmp2cata_10.1 | 37266 | 5.3 | 166 | 4 | 49 | 128 | 247 | 0.01 | 11.82 | 0.23 | 0.75 | 0.32 | 5.7 | 22.2 | 44.6 | 108 | 10370 | 0.47 | 394 | 6.8 | 0.1 | 743 | 4.76 | 0.66 |
| qmp2cata_16 | | 5.5 | | | | | | | | | | | | | | | | | | | | | 4.83 | 0.66 |

(*continued*)

TABLE 2. SUMMARY OF YERINGTON ZIRCON ANALYTICAL RESULTS (*continued*)

| | Laser Raman | | Age | | | | | | | | | | | | | | | | | | | | Oxygen | |
|---|---|---|---|---|---|---|---|---|---|---|---|---|---|---|---|---|---|---|---|---|---|---|---|---|
| Analysis | Amplitude (counts) | FWHM ($cm^{-1}$) | $^{206}Pb/^{238}U$ (Ma) | 1σ | Th (ppm) | U (ppm) | Y (ppm) | La (ppm) | Ce (ppm) | Nd (ppm) | Sm (ppm) | Eu (ppm) | Gd (ppm) | Dy (ppm) | Er (ppm) | Yb (ppm) | Hf (ppm) | $Eu_N/Eu_N^*$ | $Ce_N/Ce_N^*$ | Ti (ppm) | Fe (ppm) | T (°C) | $\delta^{18}O$ (‰) | 2σ total |
| Jgp3 | | | | | | | | | | | | | | | | | | | | | | | | |
| qmp3_5.1 | 15240 | 5.6 | 168 | 3 | 98 | 224 | 568 | 0.11 | 28.11 | 0.68 | 1.66 | 1.04 | 13.6 | 45.7 | 97.5 | 221 | 9292 | 0.67 | 230 | 5.9 | 0.4 | 729 | | |
| qmp3_6.1 | 10893 | 5.8 | 170 | 3 | 159 | 301 | 1238 | 0.06 | 34.53 | 2.33 | 7.05 | 4.45 | 56.8 | 141.1 | 160.4 | 226 | 10150 | 0.68 | 103 | 10.7 | 11.7 | 787 | 5.05 | 0.67 |
| qmp3_7.1 | 11718 | 9.4 | 171 | 1 | 1137 | 1142 | 1646 | 0.10 | 84.78 | 4.41 | 7.81 | 4.44 | 48.2 | 154.7 | 277.1 | 569 | 8129 | 0.70 | 78 | 8.5 | 0.4 | 765 | | |
| qmp3_8.1 | 13093 | 6.2 | 169 | 1 | 272 | 435 | 375 | 0.02 | 27.36 | 0.50 | 1.12 | 0.65 | 8.7 | 30.4 | 66.6 | 160 | 10049 | 0.63 | 288 | 5.9 | 0.6 | 730 | | |
| qmp3_12 | | | | | | | | | | | | | | | | | | | | | | | 4.44 | 0.67 |
| qmp3_16 | | | | | | | | | | | | | | | | | | | | | | | 5.04 | 0.67 |
| qmp3_17.1 | 36075 | 6.6 | 168 | 2 | 119 | 256 | 465 | 0.05 | 26.72 | 0.40 | 1.20 | 0.52 | 10.9 | 40.9 | 81.1 | 176 | 10429 | 0.44 | 475 | 7.1 | 1.1 | 748 | | |
| qmp3_18.1 | 29040 | 6.5 | 171 | 3 | 168 | 256 | 696 | 0.01 | 28.88 | 1.49 | 2.92 | 1.04 | 21.6 | 67.2 | 121.4 | 238 | 10060 | 0.40 | 87 | 7.6 | 0.2 | 754 | | |
| qmp3_19.1 | 49568 | 5.6 | 167 | 3 | 280 | 407 | 986 | 0.02 | 40.88 | 2.09 | 4.32 | 1.64 | 28.7 | 97.2 | 176.7 | 347 | 10398 | 0.45 | 93 | 6.4 | 0.2 | 738 | 5.14 | 0.66 |
| qmp3_20.1 | 49312 | 5.9 | 173 | 1 | 410 | 517 | 1044 | 0.07 | 61.17 | 3.17 | 5.56 | 2.60 | 32.2 | 98.0 | 181.2 | 372 | 8152 | 0.59 | 78 | 8.6 | 0.7 | 766 | | |
| Jgp3 (TA/CA) | | | | | | | | | | | | | | | | | | | | | | | | |
| qmp3cata_1.1 | 17582 | 6.1 | 171 | 1 | 160 | 342 | 326 | 0.01 | 22.79 | 0.38 | 0.87 | 0.41 | 7.1 | 27.0 | 58.8 | 140 | 10657 | 0.50 | 321 | 6.2 | 0.5 | 735 | | |
| qmp3cata_2.1 | 53575 | 5.6 | 171 | 2 | 462 | 530 | 346 | 0.01 | 35.68 | 0.62 | 1.31 | 0.79 | 9.8 | 31.3 | 58.9 | 125 | 9887 | 0.67 | 283 | 6.4 | 0.4 | 737 | 4.74 | 0.67 |
| qmp3cata_3.1 | 22634 | 5.4 | 173 | 2 | 575 | 684 | 530 | 0.01 | 45.87 | 0.74 | 1.94 | 0.98 | 13.9 | 48.4 | 93.2 | 209 | 10247 | 0.57 | 375 | 6.7 | 0.2 | 741 | | |
| qmp3cata_4.1 | 7343 | 5.5 | 168 | 3 | 44 | 126 | 165 | 0.01 | 10.96 | 0.25 | 0.56 | 0.31 | 3.5 | 13.6 | 29.6 | 72 | 10651 | 0.67 | 233 | 3.5 | 0.3 | 685 | | |
| qmp3cata_6.1 | 3878 | 6.1 | 168 | 1 | 212 | 350 | 493 | 0.02 | 21.53 | 1.22 | 2.26 | 1.08 | 15.0 | 47.1 | 84.2 | 188 | 9827 | 0.57 | 75 | 4.6 | 0.4 | 708 | 4.30 | 0.66 |
| qmp3cata_7.1 | 46867 | 5.1 | 167 | 2 | 149 | 305 | 417 | 0.14 | 22.08 | 0.63 | 1.30 | 0.71 | 9.7 | 35.4 | 72.9 | 171 | 9823 | 0.61 | 167 | 4.8 | 0.5 | 712 | | |
| qmp3cata_10.1 | 50672 | 5.3 | 170 | 2 | 108 | 245 | 255 | 0.02 | 14.41 | 0.29 | 0.77 | 0.42 | 5.1 | 19.2 | 46.1 | 129 | 9732 | 0.64 | 307 | 4.2 | 0.7 | 700 | | |
| Jbqm | | | | | | | | | | | | | | | | | | | | | | | | |
| bqm_1.1 | 48644 | 5.8 | 167 | 3 | 120 | 168 | 678 | 0.01 | 19.82 | 2.36 | 5.09 | 1.26 | 25.3 | 72.8 | 108.1 | 197 | 9796 | 0.34 | 42 | 15.2 | 0.1 | 824 | 5.69 | 0.64 |
| bqm_2.1 | 65238 | 5.7 | 170 | 2 | 107 | 178 | 577 | 0.01 | 19.17 | 1.31 | 2.88 | 0.93 | 20.7 | 62.9 | 98.1 | 193 | 11432 | 0.37 | 74 | 9.9 | 0.2 | 780 | 5.88 | 0.67 |
| bqm_3.1 | 40608 | 6.7 | 168 | 2 | 64 | 104 | 353 | 0.01 | 13.27 | 0.42 | 1.33 | 0.55 | 10.5 | 37.0 | 58.7 | 112 | 10130 | 0.45 | 228 | 15.9 | 0.2 | 829 | | |
| bqm_4.1 | 38612 | 7.0 | 166 | 1 | 241 | 315 | 1043 | 0.09 | 25.16 | 4.56 | 6.01 | 1.68 | 33.6 | 96.7 | 178.0 | 321 | 8905 | 0.36 | 17 | 23.0 | 0.1 | 871 | | |
| bqm_5.1 | | | | | | | | | | | | | | | | | | | | | | | 5.28 | 0.66 |
| bqm_6.1 | 57445 | 5.6 | 168 | 2 | 183 | 263 | 884 | 0.01 | 32.60 | 1.74 | 4.29 | 1.12 | 30.4 | 93.8 | 146.9 | 267 | 11374 | 0.30 | 107 | 8.7 | 39.7 | 767 | 5.46 | 0.66 |
| bqm_7.1 | 43454 | 6.4 | 171 | 3 | 119 | 434 | 208 | 0.40 | 18.30 | 0.20 | 0.36 | 0.11 | 3.3 | 16.5 | 39.5 | 102 | 14219 | 0.30 | 365 | 7.0 | 4.7 | 745 | 5.58 | 0.65 |
| bqm_8.1 | 63554 | 6.0 | 171 | 2 | 67 | 227 | 199 | 0.01 | 17.62 | 0.17 | 0.48 | 0.13 | 3.8 | 18.5 | 36.1 | 77 | 12666 | 0.28 | 660 | 6.5 | 0.6 | 739 | | |
| bqm_9.1 | 41465 | 5.9 | 172 | 2 | 219 | 364 | 731 | 0.01 | 25.42 | 0.77 | 2.39 | 0.67 | 20.3 | 73.1 | 127.6 | 245 | 12764 | 0.29 | 235 | 8.3 | 0.2 | 762 | 5.27 | 0.67 |
| bqm_10 | | | | | | | | | | | | | | | | | | | | | | | 5.23 | 0.66 |
| bqm_11 | | | | | | | | | | | | | | | | | | | | | | | 5.69 | 0.66 |
| bqm_12 | | | | | | | | | | | | | | | | | | | | | | | 4.94 | 0.67 |
| bqm_13 | | 6.1 | | | | | | | | | | | | | | | | | | | | | 5.64 | 0.65 |
| Jbqm (TA/CA) | | | | | | | | | | | | | | | | | | | | | | | | |
| bqmcata_1.1 | 58117 | 5.8 | 229 | 3 | 87 | 313 | 796 | 0.00 | 10.56 | 0.33 | 1.01 | 0.33 | 12.4 | 60.7 | 155.1 | 369 | 9846 | 0.28 | 226 | 18.8 | 0.2 | 848 | | |
| bqmcata_2.1 | | | | | | | | | | | | | | | | | | | | | | | 4.93 | 0.69 |
| bqmcata_9.1 | 15551 | 5.9 | 231 | 4 | 66 | 210 | 588 | 0.01 | 9.90 | 0.31 | 0.90 | 0.27 | 9.7 | 51.4 | 112.8 | 237 | 9522 | 0.27 | 219 | 9.0 | 0.5 | 770 | | |
| bqmcata_10.1 | 24091 | 6.8 | 174 | 3 | 70 | 967 | 86 | 0.01 | 13.47 | 0.04 | 0.16 | 0.04 | 1.3 | 6.0 | 16.0 | 51 | 15267 | 0.27 | 3313 | 3.3 | 2.5 | 680 | | |
| bqmcata_11.1 | 36348 | 5.4 | 167 | 2 | 51 | 92 | 320 | 0.01 | 14.96 | 0.40 | 1.26 | 0.56 | 9.2 | 32.1 | 52.7 | 108 | 9678 | 0.50 | 273 | 18.8 | 0.2 | 848 | 5.69 | 0.68 |
| bqmcata_12.1 | 20578 | 5.7 | 169 | 2 | 113 | 222 | 329 | 0.00 | 16.29 | 0.63 | 1.40 | 0.39 | 9.9 | 32.7 | 55.5 | 110 | 10835 | 0.32 | 133 | 21.5 | 0.6 | 863 | 5.24 | 0.67 |
| bqmcata_13.1 | 17050 | 6.6 | 171 | 1 | 383 | 516 | 1070 | 0.04 | 27.92 | 3.46 | 5.17 | 1.31 | 28.3 | 99.7 | 187.1 | 341 | 10195 | 0.33 | 28 | 13.6 | 0.2 | 813 | 4.99 | 0.66 |
| bqmcata_14.1 | 34001 | 5.2 | 173 | 4 | 55 | 108 | 293 | 0.01 | 14.22 | 0.39 | 1.00 | 0.36 | 7.2 | 29.3 | 50.8 | 103 | 9836 | 0.40 | 218 | 15.1 | 0.2 | 824 | 5.52 | 0.67 |
| bqmcata_15.1 | 63856 | 5.6 | 173 | 2 | 66 | 118 | 298 | 0.36 | 18.26 | 0.50 | 1.09 | 0.41 | 8.6 | 30.0 | 52.4 | 101 | 10434 | 0.41 | 182 | 27.5 | 30.1 | 893 | | |

(*continued*)

TABLE 2. SUMMARY OF YERINGTON ZIRCON ANALYTICAL RESULTS (*continued*)

| | Laser Raman | | Age | | | | | | | | | | | | | | | | | | | Oxygen | |
|---|---|---|---|---|---|---|---|---|---|---|---|---|---|---|---|---|---|---|---|---|---|---|---|
| Analysis | Amplitude (counts) | FWHM ($cm^{-1}$) | $^{206}Pb/^{238}U$ (Ma) | 1σ | Th (ppm) | U (ppm) | Y (ppm) | La (ppm) | Ce (ppm) | Nd (ppm) | Sm (ppm) | Eu (ppm) | Gd (ppm) | Dy (ppm) | Er (ppm) | Yb (ppm) | Hf (ppm) | $Eu_N/Eu_N^*$ | $Ce_N/Ce_N^*$ | Ti (ppm) | Fe (ppm) | T (°C) | $\delta^{18}O$ (‰) | 2σ total |
| Jpg | | | | | | | | | | | | | | | | | | | | | | | | |
| pqm_2.1 | 19353 | 5.7 | 169 | 2 | 171 | 353 | 364 | 0.02 | 20.26 | 0.62 | 1.34 | 0.66 | 8.0 | 28.1 | 63.5 | 162 | 10174 | 0.62 | 160 | 5.6 | 0.6 | 725 | | |
| pqm_5.1 | 5276 | 6.6 | 170 | 1 | 390 | 1293 | 316 | 0.02 | 18.19 | 0.29 | 0.50 | 0.38 | 3.9 | 18.3 | 57.7 | 200 | 10640 | 0.82 | 244 | 3.1 | 0.8 | 676 | | |
| pqm_6.1 | 18484 | 6.3 | 167 | 2 | 262 | 423 | 720 | 0.03 | 28.13 | 1.98 | 3.32 | 1.44 | 20.2 | 66.2 | 124.2 | 279 | 10117 | 0.54 | 55 | 5.4 | 1.1 | 721 | 5.72 | 0.67 |
| pqm_7 | | | | | | | | | | | | | | | | | | | | | | | 4.93 | 0.66 |
| pqm_8 | | | | | | | | | | | | | | | | | | | | | | | 4.82 | 0.68 |
| pqm_9.1 | 14750 | 6.7 | 171 | 2 | 312 | 503 | 545 | 0.03 | 30.47 | 0.73 | 1.60 | 0.70 | 11.1 | 41.7 | 97.9 | 259 | 10004 | 0.50 | 210 | 5.8 | 3.0 | 729 | | |
| pqm_10.1 | 13756 | 7.9 | 452 | 7 | 81 | 138 | 951 | 0.16 | 11.49 | 0.94 | 2.21 | 0.92 | 20.2 | 87.9 | 175.8 | 347 | 7842 | 0.42 | 66 | 19.9 | 35.3 | 855 | 5.99 | 0.70 |
| pqm_11 | | | | | | | | | | | | | | | | | | | | | | | 5.52 | 0.67 |
| pqm_12 | | | | | | | | | | | | | | | | | | | | | | | 4.99 | 0.67 |
| pqm_13 | | | | | | | | | | | | | | | | | | | | | | | 5.26 | 0.66 |
| pqm_14 | | 6.3 | | | | | | | | | | | | | | | | | | | | | 5.46 | 0.69 |
| Jpg (TA/CA) | | | | | | | | | | | | | | | | | | | | | | | | |
| pqmcata_1.1 | 868 | 3.6 | 171 | 2 | 115 | 250 | 318 | 0.01 | 23.42 | 0.30 | 0.86 | 0.35 | 7.8 | 29.0 | 57.5 | 118 | 10671 | 0.41 | 530 | 7.4 | 0.2 | 751 | | |
| pqmcata_2.1 | 8678 | 5.7 | 168 | 6 | 45 | 132 | 196 | 0.00 | 14.20 | 0.15 | 0.63 | 0.20 | 4.0 | 16.1 | 35.1 | 80 | 10982 | 0.38 | 984 | 9.7 | 0.7 | 778 | 5.16 | 0.65 |
| pqmcata_3.1 | 9953 | 5.5 | 163 | 2 | 107 | 212 | 494 | 0.15 | 24.16 | 0.55 | 1.35 | 0.52 | 11.1 | 42.9 | 88.4 | 188 | 9637 | 0.41 | 245 | 9.4 | 0.5 | 775 | | |
| pqmcata_6.1 | 19105 | 4.9 | 167 | 2 | 71 | 171 | 184 | 0.01 | 10.73 | 0.18 | 0.57 | 0.30 | 4.2 | 14.7 | 32.3 | 85 | 10832 | 0.60 | 431 | 3.4 | 0.3 | 682 | | |
| pqmcata_8.1 | 16556 | 5.5 | 169 | 2 | 219 | 379 | 464 | 0.02 | 22.29 | 1.07 | 1.97 | 0.58 | 13.5 | 45.5 | 79.8 | 166 | 10446 | 0.34 | 89 | 8.0 | 0.5 | 759 | | |
| Jqmd | | | | | | | | | | | | | | | | | | | | | | | | |
| gd_1.1 | 19662 | 6.5 | 168 | 1 | 1450 | 886 | 2589 | 0.09 | 90.33 | 5.89 | 11.98 | 4.54 | 94.3 | 277.8 | 431.8 | 748 | 8526 | 0.41 | 72 | 26.2 | 0.2 | 887 | 5.88 | 0.69 |
| gd_2.1 | 935 | 6.8 | 163 | 4 | 88 | 230 | 359 | 0.05 | 16.03 | 0.32 | 1.04 | 0.28 | 7.5 | 31.5 | 65.3 | 150 | 12280 | 0.30 | 387 | 28.7 | 70.0 | 898 | | |
| gd_3.1 | 6952 | 6.4 | 171 | 2 | 351 | 389 | 1155 | 0.02 | 29.31 | 2.80 | 5.86 | 1.60 | 38.5 | 120.3 | 197.1 | 367 | 10589 | 0.32 | 51 | 12.2 | 1.1 | 801 | | |
| gd_4.1 | 11467 | 7.0 | 171 | 1 | 709 | 716 | 1822 | 0.06 | 38.34 | 3.99 | 7.57 | 2.17 | 49.4 | 180.0 | 309.2 | 564 | 10351 | 0.34 | 42 | 13.4 | 2.4 | 811 | | |
| gd_5.1 | 3943 | 7.4 | 170 | 1 | 547 | 594 | 1838 | 0.26 | 43.71 | 4.24 | 7.55 | 2.35 | 54.7 | 181.1 | 306.8 | 569 | 10121 | 0.35 | 42 | 14.8 | 8.6 | 821 | | |
| gd_15 | | | | | | | | | | | | | | | | | | | | | | | 5.56 | 0.65 |
| Jqmd (TA/CA) | | | | | | | | | | | | | | | | | | | | | | | | |
| gdcata_2.1 | 19468 | 5.9 | 172 | 3 | 227 | 459 | 997 | 0.02 | 25.97 | 2.38 | 4.60 | 1.45 | 32.2 | 99.5 | 167.7 | 313 | 11261 | 0.36 | 49 | 12.3 | 0.9 | 802 | | |
| gdcata_3.1 | 13243 | 7.7 | 104 | 1 | 1466 | 2189 | 1690 | 0.06 | 9.92 | 2.78 | 4.61 | 0.78 | 33.6 | 148.5 | 300.4 | 622 | 10135 | 0.19 | 14 | 9.8 | 0.7 | 779 | | |
| gdcata_4.1 | 22383 | 7.9 | 101 | 1 | 1717 | 1702 | 1137 | 0.04 | 13.79 | 1.68 | 3.29 | 0.67 | 26.0 | 97.7 | 201.5 | 421 | 8632 | 0.22 | 37 | 14.1 | 0.6 | 816 | 6.23 | 0.67 |
| gdcata_6 | | | | | | | | | | | | | | | | | | | | | | | 5.14 | 0.67 |
| gdcata_7.1 | 4077 | 6.7 | 173 | 2 | 875 | 737 | 2386 | 0.08 | 52.85 | 5.37 | 10.00 | 3.38 | 81.1 | 246.8 | 389.5 | 688 | 9464 | 0.36 | 42 | 16.4 | 0.2 | 833 | | |
| gdcata_11.1 | 3910 | 7.5 | 175 | 2 | 1860 | 1100 | 4191 | 0.11 | 100.16 | 8.54 | 21.45 | 7.73 | 164.4 | 464.0 | 673.3 | 1129 | 8862 | 0.40 | 68 | 28.0 | 0.2 | 895 | | |
| Mount Dromedary | | | | | | | | | | | | | | | | | | | | | | | | |
| MtD_27.2 | 8946 | 10.0 | 103 | 2 | 1375 | 1535 | 2214 | 0.09 | 8.61 | 2.73 | 5.84 | 1.72 | 62.7 | 213.2 | 382.8 | 724 | 8019 | 0.27 | 16 | 15.4 | 0.2 | 826 | 6.54 | 0.67 |
| MtD_28.1 | 39378 | 6.4 | 97 | 1 | 125 | 360 | 435 | 0.01 | 4.13 | 0.56 | 1.22 | 0.31 | 9.3 | 34.7 | 80.3 | 193 | 8101 | 0.28 | 37 | 15.3 | 0.3 | 825 | 6.83 | 0.66 |
| MtD_29.1 | 27370 | 6.7 | 101 | 1 | 372 | 505 | 1061 | 0.07 | 6.71 | 2.75 | 4.59 | 1.15 | 33.8 | 104.6 | 181.3 | 356 | 8019 | 0.28 | 9 | 17.2 | 0.3 | 838 | 6.47 | 0.67 |
| MtD_31.2 | 52781 | 6.9 | 96 | 1 | 224 | 348 | 729 | 0.02 | 5.47 | 1.77 | 3.43 | 0.75 | 22.3 | 74.6 | 126.0 | 246 | 8677 | 0.26 | 14 | 12.2 | 0.9 | 801 | 7.05 | 0.69 |
| Mount Dromedary (TA/CA) | | | | | | | | | | | | | | | | | | | | | | | | |
| MtDC_24.1 | 6037 | 6.8 | 100 | 1 | 68 | 184 | 229 | 0.00 | 3.19 | 0.20 | 0.58 | 0.13 | 4.4 | 20.3 | 42.3 | 102 | 9257 | 0.25 | 107 | 9.3 | 0.1 | 773 | | |
| MtDC_25.1 | 32636 | 6.1 | 99 | 2 | 112 | 358 | 297 | 0.00 | 4.23 | 0.20 | 0.68 | 0.15 | 5.2 | 24.7 | 55.6 | 135 | 10571 | 0.24 | 169 | 8.2 | 0.3 | 761 | 6.52 | 0.66 |
| MtDC_26.2 | 44230 | 6.3 | 100 | 2 | 279 | 442 | 707 | 0.02 | 4.59 | 1.34 | 3.03 | 0.71 | 20.5 | 70.5 | 119.9 | 236 | 8904 | 0.28 | 18 | 11.4 | 0.3 | 794 | 6.35 | 0.66 |
| MtDC_27.1 | 40306 | 6.7 | 100 | 1 | 254 | 653 | 459 | 0.01 | 6.07 | 0.40 | 1.16 | 0.22 | 9.6 | 37.8 | 82.9 | 200 | 10044 | 0.20 | 104 | 9.3 | 0.4 | 773 | 6.28 | 0.68 |

*Note:* Abbreviations: FWHM—full width half maximum; TA/CA—thermal annealing and chemical abrasion.

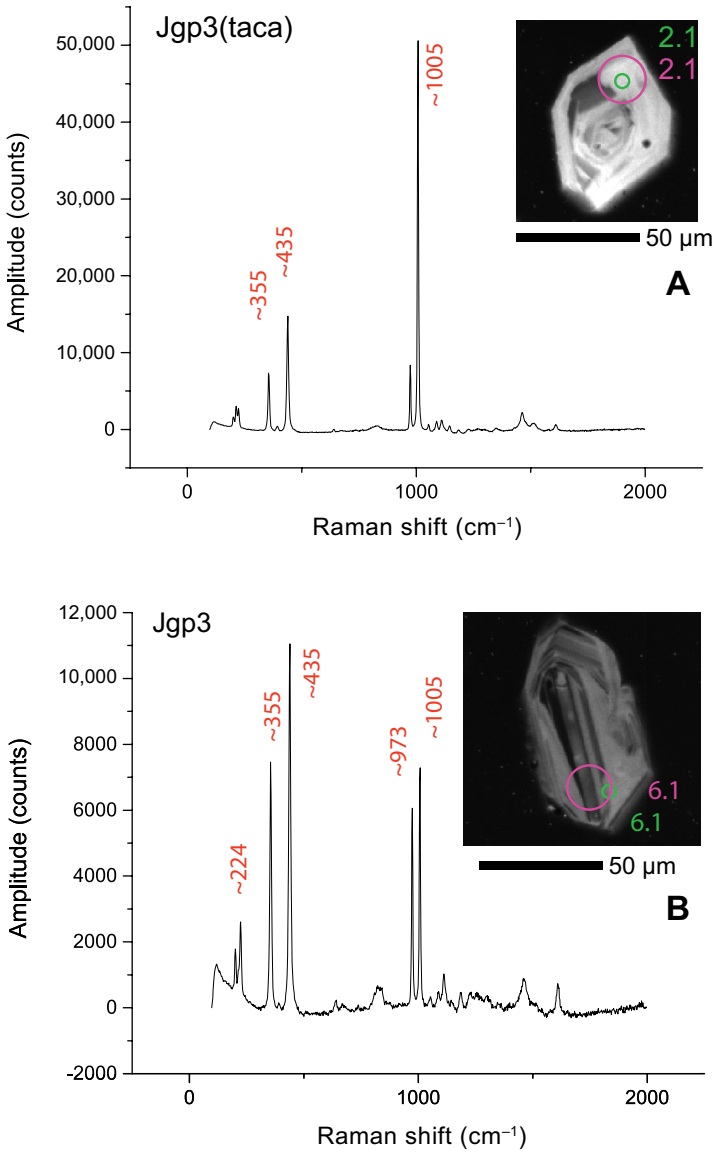


**Figure 3. (A) An example of a Raman spectrum from analysis Jgp3cata_2.1, a thermally annealed and chemically abraded zircon from sample Jgp3. Raman analytical spot (small green circle) analysis guided combined U-Pb + trace element (TE) spot (large purple circle) choice. Peaks of structurally intact zircons occur at ~335, ~435, and ~1005 cm$^{-1}$, which correspond to $SiO_4$, $SiO_4$, and Zr-Si bands. (B) An example of a metamict Raman spectrum from analysis Jgp3_6.1, an untreated zircon from sample Jgp3. Note the lower intensity of the main ~1005 cm$^{-1}$ peak, indicating degradation in the zircon crystal structure. Images are cathodoluminescence.**

## Trace Element Analyses

Results are reported in Table 2 and Figures 5–7. Trace element concentrations do not vary systematically between untreated and treated zircons, and results are pooled. The majority (>90%) of analyzed Yerington zircons have U contents between 90 and 500 ppm; only six of 110 grains analyzed were over 1000 ppm U (three of those are from sample Jqmd) (Fig. 6). Th/U ratios are dominantly between 0.25 and 0.75, with <20% of analyses >0.75 and only 1 analysis <0.25. Rare earth element values vary over 2 orders of magnitude between samples. Intra-sample REE variability is ~1 order of magnitude—similar to data reported by Dilles et al., 2015—which is typical of zircon populations (e.g., Hoskin and Schaltegger, 2003; Hanchar and van Westrenen, 2007). Sample Jqmd has the highest overall concentration of REE, while Jgp2 has the lowest. There are no systematic variations in REE concentrations between host units and porphyry dike units. $Ce_N/Ce_N^*$ values are mostly <400 (avg. 205 ± 192 (1σ)), with 12 analyses >400 (Figs. 6 and 7). Only one grain had a $Ce_N/Ce_N^*$ value >1000, but it also had unusually high Sm/Nd and is therefore not considered reliable. $Eu_N/Eu_N^*$ ratios range from 0.19 to 1.05 and average 0.45 ± 0.14 (1σ). Twenty grains (eight from Jpg2 and 8 from Jpg3) have $Eu_N/Eu_N^*$>0.60 (Figs. 6 and 7). $Ce_N/Ce_N^*$ values show little correlation with $Eu_N/Eu_N^*$ values (Fig. 7). The Ce/U varies proportionally with $Eu_N/Eu_N^*$ when $Eu_N/Eu_N^*$<~0.4 and inversely with $Eu_N/Eu_N^*$ when $Eu_N/Eu_N^*$>~0.4 (Fig. 7). U/Yb exhibits the opposite trend against $Eu_N/Eu_N^*$ (Fig. 7). Hf concentrations range from ~8500–15,000 ppm (average 10,095 ± 1155 [1σ] ppm) in host units Jqmd and Jbqm (Fig. 7). Ti concentrations range from 3 to 29 ppm with an average of 9.8 ± 5.6 (1σ) ppm (Figs. 6 and 7). Host units Jqmd and Jbqm have higher average values (17.6 and 13.1 ppm Ti, respectively) than the porphyry dike units. Host unit Jpg has Ti (<10 ppm), similar to the porphyry dike units than to the other host units. $Eu_N/Eu_N^*$ decreases with decreasing Ti and increasing Hf in the early samples; in later samples, $Eu_N/Eu_N^*$ increases with decreasing Ti (Fig. 6). When emplacement order based on field relations is considered (host units earlier than porphyry dikes; oldest dike is Jgp1 and youngest is Jgp3), the Yerington zircons show decreasing Ti concentration with time. Model Ti-in-zircon crystallization temperatures (Ferry and Watson, 2007) were calculated assuming activity ($a$) of titania and silica fixed at $a_{TiO_2}$ = 0.7 and $a_{SiO_2}$ = 1, based on estimates from Ghiorso and Gualda (2013) and McDowell et al. (2014), which allows for direct comparison with data from Dilles et al. (2015). Calculated temperatures indicate an overall decrease in temperature corresponding to the drop in Ti concentration during zircon crystallization (Fig. 6).

## Oxygen Isotope Analyses

With the exception of 5 of 92 points analyzed, which were excluded due to measured $\delta^{18}O$ being lower than the external error, all of the individual zircon spot analyses from Yerington units were reproducible within external error (2σ SE). Units Jqmd, Jbqm, and Jpg have mean $\delta^{18}O$ values of 5.7 ± 0.5‰, 5.4 ± 0.3‰, and 5.3 ± 0.4‰, respectively (all reported at 1σ standard devia-

TABLE 3. SUMMARY OF ANALYSES OF TA/CA TREATED AND UNTREATED YERINGTON ZIRCON

| Sample | Description | Age (Ma) | 2σ | $\delta^{18}O$ (‰) | 1σ s.d. | $Eu_N/Eu_N^*$ | $Ce_N/Ce_N^*$ | Ti (ppm) | FWHM ($cm^{-1}$) |
|---|---|---|---|---|---|---|---|---|---|
| Jqmd | Untreated | 169.6 | 1.5 | 5.7 | 0.2 | 119 | 0.35 | 19.1 | 6.82 |
| Jqmd | Treated | 173.6 | 2.1 | 5.7 | 0.8 | 42 | 0.29 | 16.0 | 7.12 |
| Jqmd | Combined | 170.0 | 1.4 | 5.7 | 0.5 | 80 | 0.33 | 17.6 | 6.97 |
| Jbqm | Untreated | 168.9 | 1.5 | 5.5 | 0.3 | 152 | 0.34 | 11.8 | 6.14 |
| Jbqm | Treated | 170.9 | 1.9 | 5.3 | 0.3 | 179 | 0.35 | 12.5 | 5.87 |
| Jbqm | Combined | 169.6 | 1.3 | 5.4 | 0.3 | 167 | 0.34 | 12.1 | 6.00 |
| Jpg | Untreated | 169.4 | 1.9 | 5.3 | 0.4 | 146 | 0.58 | 8.0 | 6.32 |
| Jpg | Treated | 169.4 | 2.0 | 5.2 | — | 455 | 0.43 | 7.6 | 5.03 |
| Jpg | Combined | 169.4 | 1.5 | 5.3 | 0.4 | 301 | 0.50 | 7.8 | 5.83 |
| Jgp1 | Untreated | 169.3 | 1.4 | 5.6 | 0.4 | 152 | 0.47 | 10.2 | 6.23 |
| Jgp1 | Treated | 167.0 | 1.9 | 5.6 | 0.3 | 117 | 0.43 | 12.0 | 6.01 |
| Jgp1 | Combined | 169.0 | 1.2 | 5.6 | 0.4 | 134 | 0.45 | 11.1 | 6.11 |
| Jgp1.5 | Untreated | 168.6 | 1.5 | 5.5 | 0.4 | 396 | 0.50 | 7.6 | 6.09 |
| Jgp1.5 | Treated | 168.9 | 1.5 | 4.1 | 1.0 | 183 | 0.43 | 7.8 | 5.53 |
| Jgp1.5 | Combined | 168.7 | 1.1 | 5.3 | 0.7 | 289 | 0.46 | 7.7 | 5.80 |
| Jgp2 | Untreated | 169.8 | 1.7 | 5.3 | 0.2 | 160 | 0.60 | 5.5 | 5.90 |
| Jgp2 | Treated | 169.3 | 1.8 | 4.5 | 0.4 | 237 | 0.51 | 6.5 | 5.47 |
| Jgp2 | Combined | 169.6 | 1.3 | 5.0 | 0.5 | 201 | 0.55 | 6.0 | 5.68 |
| Jgp3 | Untreated | 170.1 | 1.4 | 4.9 | 0.3 | 137 | 0.57 | 7.6 | 6.45 |
| Jgp3 | Treated | 169.4 | 1.5 | 4.5 | 0.3 | 251 | 0.60 | 5.2 | 5.60 |
| Jgp3 | Combined | 169.8 | 1.1 | 4.8 | 0.4 | 194 | 0.59 | 6.5 | 6.05 |
| Mount Dromedary | Untreated | 98.0 | 4.7 | 6.7 | 0.3 | 19 | 0.27 | 15.0 | 7.20 |
| Mount Dromedary | Treated | 100.0 | 1.6 | 6.4 | 0.1 | 99 | 0.24 | 9.5 | 6.37 |
| Mount Dromedary | Combined | 98.7 | 2.0 | 6.6 | 0.3 | 59 | 0.26 | 12.3 | 6.65 |

*Note*: Abbreviations: FWHM—full width half maximum; TA/CA—thermal annealing and chemical abrasion.

tion [s.d.]); $\delta^{18}O$ for dikes range from 4.8‰ to 5.6‰ (sample means; Fig. 8). Jgp1 and Jgp1.5, the earliest dikes to be emplaced, have mean $\delta^{18}O$ values of 5.6 ± 0.4‰ (analyses range from 5.2‰ to 6.0‰, with one outlier at 4.6‰) and 5.3 ± 0.7‰ (analyses range from 3.4‰ to 6.0‰), respectively. Mean $\delta^{18}O$ values for Jgp2 and Jgp3 were 5.0 ± 0.5‰ and 4.8 ± 0.4‰, respectively. Every sample had smaller sample sizes for treated grains than untreated grains due to increased surface topography and therefore decreased availability of viable analytical surfaces on treated grains. The oxygen isotopes for TA/CA treated grains from Jgp2 are $^{18}O$-depleted relative to untreated grains from the same sample but within external error. All other samples with treated and untreated grains yielded $\delta^{18}O$ values that were very similar. We therefore pooled the results from treated and untreated subsets of each sample for further analysis.

## DISCUSSION

### Effect of TA/CA Treatment on Zircon Analytical Results

Mount Dromedary zircon standard grains that underwent TA/CA treatment yielded more reproducible results, and the weighted average of four treated grains is 100 ± 1.7 Ma (2σ; MSWD = 0.08) with U concentrations ranging from 200 to 700 ppm. Differences in age between untreated and treated grains from the Yerington samples are not resolvable at the 2σ level (Table 3), with the exception of sample Jqmd. It should be noted that on average, the treated sample subsets have slightly lower calculated standard error compared to their untreated counterparts, but the calculated weighted-mean ages are not statistically resolvable at the 2σ level (Table 3). We therefore prefer the combined age of the treated and untreated samples, and we attribute the increased scatter for the treated grains to be an artifact of relatively small sample size. Mount Dromedary is the only exception to this with the untreated 2σ standard error of ± 4.7 m.y., compared to the ±1.6 m.y. for the treated grains.

One potential reason for the lack of improved age precision for Yerington zircon that underwent TA/CA treatment compared to the untreated aliquot of each sample could be that the U concentration is <500 ppm for the majority of the Yerington batholith zircons analyzed in this study, although higher values were reported by Dilles and Wright (1988). Therefore, the likelihood of radiation damage in the zircon crystal lattice due to U decay is considerably lower compared to high-U zircons reported in other mineralized deposits (e.g., >2000 ppm; Wang et al., 2014). With relatively few potentially metamict areas removed during TA/CA treatment as compared to the untreated grains, there is little difference in age between treated and untreated grains. The agreement

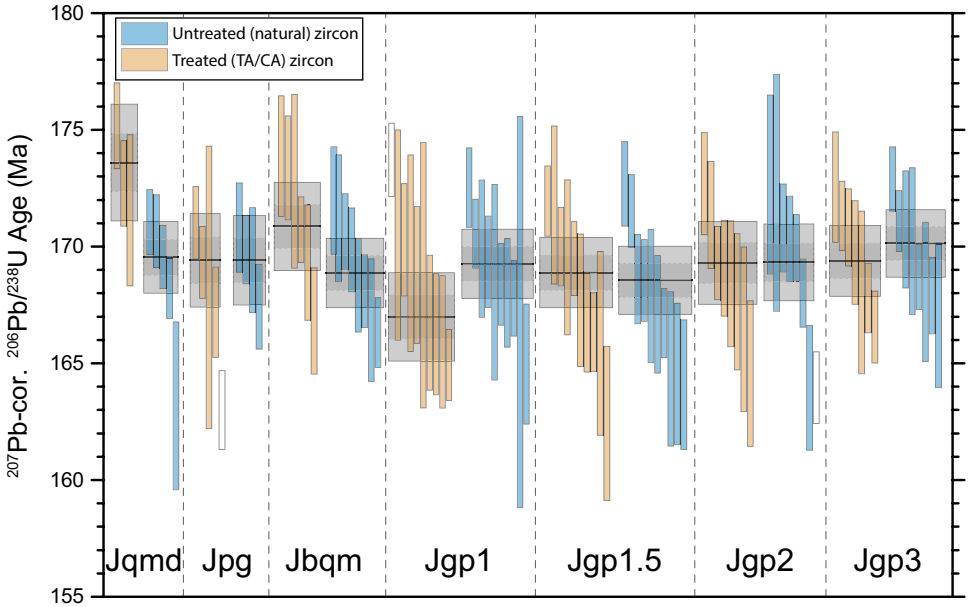


**Figure 4. Zircon U-Pb spot analyses per Yerington sample. Gray boxes denote 1σ (small box) and 2σ (large box) errors. Weighted-mean sample ages are horizontal black bars.**

between treated and untreated ages may result from our preselection of analytical spots via the laser Raman analyses. By performing the laser Raman analyses prior to SHRIMP-RG analysis, we identified potentially metamict areas and avoided them—except for those 29 grains selected to test the Raman spot-selection method (see next section)—thereby biasing our analyses toward areas of structurally intact zircon that were less affected during the TA/CA treatment. Therefore, we would expect similar results from treated and untreated grains. However, our laser Raman analyses did not reveal a distinct difference in crystallinity between the untreated compared to the treated ones, indicating that perhaps there was little overall structural damage in the Yerington samples. This is consistent with the concordant ages and small error of multi-grain zircon TIMS analyses published by Dilles and Wright (1988).

Comparison of trace element analyses of treated and untreated Yerington zircons also reveals no significant variations that are attributable to the TA/CA treatment (Fig. 5). Th/U and Ti and Hf concentrations differ between treated and untreated zircon grains in each sample but not systematically or in amounts that significantly deviate from the normal range of elemental variation in zircon from the Yerington batholith (Dilles et al., 2015) (Table 2). However, zircons are commonly sector zoned in trace element compositions, including Ti, which we did not systematically investigate in this study (cf. Lee et al., 2012; Dilles et al., 2015). Samples Jgp2, Jgp3, and Mount Dromedary show slight differences in REE patterns between treated and untreated grains—the REE concentrations for TA/CA treated Jgp2 zircon are higher than those of their untreated counterparts but still overlap the untreated concentrations (Fig. 5). Jgp3 and Mount Dromedary display treated and untreated REE patterns that overlap by ~50%, but the concentrations of treated grains are uniformly lower than those of their untreated counterparts.

There is no statistically significant difference between individual oxygen isotope spot analyses between treated and untreated zircons in Yerington samples within error (Fig. 8). This is not unexpected, because under the thermal annealing conditions utilized in this study (46 h at 850 °C), the diffusive length scale of oxygen is too small to induce $^{18}O/^{16}O$ fractionation. Rates of oxygen diffusion in zircon are variable and depend strongly on water availability, temperature (T), and pressure (P) (cf. Watson and Cherniak, 1997; Peck et al., 2003). Watson and Cherniak (1997) estimate that under dry conditions, significant perturbation of $^{18}O/^{16}O$ through a 200-µm-diameter zircon requires ~65 m.y. at 900 °C and roughly 10 k.y. under wet conditions at 850 °C. We would expect any modification of zircon $^{18}O/^{16}O$ during annealing would result from either: (1) zircon initially zoned in $^{18}O/^{16}O$ that was homogenized via internal diffusion, which should result in a systematic change between treated and untreated zircons across all samples that is not reflected in our data set; or (2) ircon exchanging O with a host of different $^{18}O/^{16}O$ composition via diffusion. A larger data set and/or higher-precision O isotope data is needed to confirm if our initial result is reproducible.

In summary, there is no statistically significant difference in U-Pb age, trace element composition, or $\delta^{18}O$ between TA/CA treated and untreated zircon

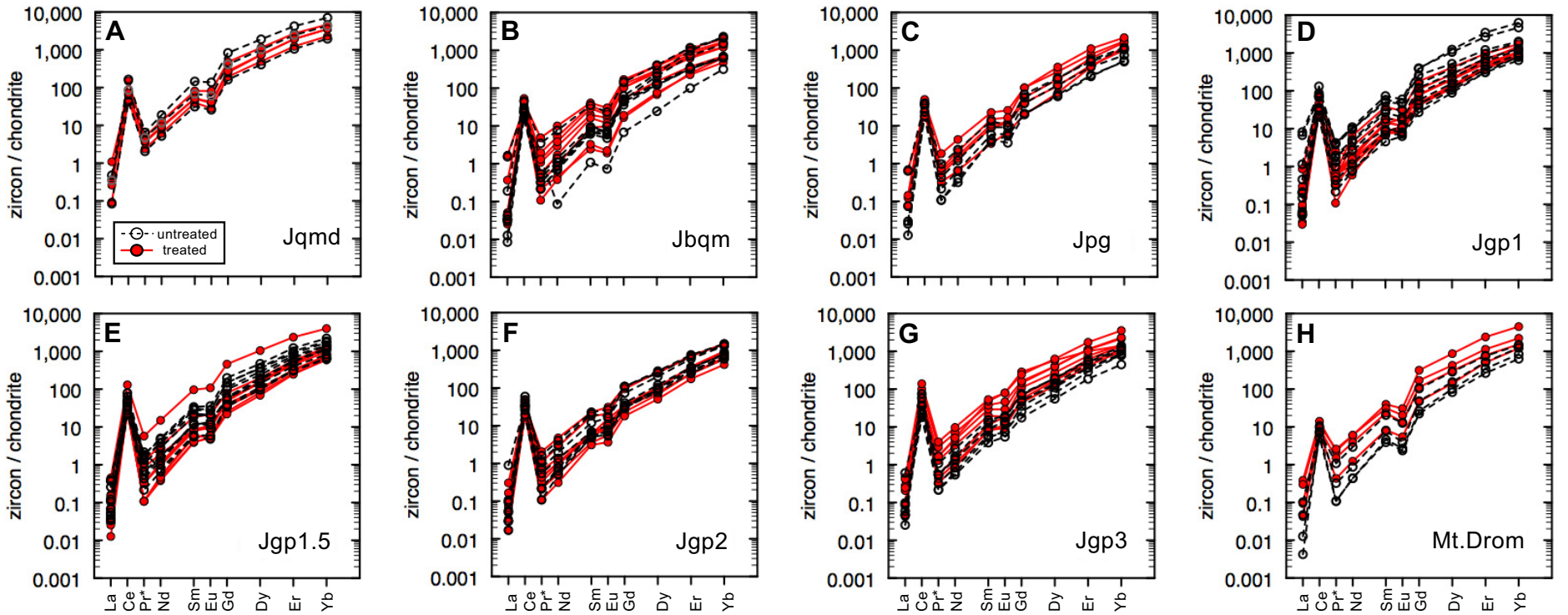


**Figure 5. Chondrite-normalized REE patterns for treated (red solid line) and untreated (black dashed line) Yerington samples and secondary standard Mount Dromedary. Normalized to C1 chondrite of McDonough and Sun (1995).**

from the same sample. Thus, it appears that for low-U samples lacking significant radiation damage, TA/CA treatment does not statistically improve precision or reproducibility for zircon U-Pb, trace element, or $\delta^{18}O$ data. The TA/CA treatment is also not detrimental to trace element and $\delta^{18}O$ analyses obtained on treated grains. All data interpretation henceforth is the combination of all treated and untreated grain analyses for a given sample.

## Assessing Utility of Laser Raman–Based Pre-Selection of Analytical Spots

Twenty-nine grains had laser Raman spectra with low FWHM on the three crystalline zircon bonding peaks and the presence of additional peaks in the spectra relative to the standards (which are assumed to be crystalline zircon). We interpret low-amplitude and additional spectral peaks to be the result of radiation damage that disordered the zircon crystalline structure or produced amorphous zones with no crystalline structure. All zircons analyzed retain characteristic crystalline zircon laser Raman peaks. We purposely analyzed these 29 grains for U-Pb age, trace element, and oxygen isotope compositions to see if grains we interpreted as metamict yielded larger errors, discordance, or differences in age relative to non-metamict grains. Twenty-eight of the 29 analyses yield U-Pb ages that are analytically indistinguishable from other grains from the same samples. A common measure of SHRIMP-RG instrument mass fractionation, UO/U (e.g., Ireland and Williams, 2003), yielded the same range of measured values (5.1–5.7) for grains with typical laser Raman spectra, grains interpreted to be metamict, and the standard Temora-2. Common Pb was also not elevated in grains interpreted to be metamict. Ten $\delta^{18}O$ analyses of grains with additional Raman peaks yielded anomalously low $\delta^{18}O$ (<3‰) when compared with other grains from the same sample. However, seven of those analytical spots were partially off the grain, which likely would have rendered them unusable due to mass fractionation problems encountered due to topography at the grain boundary. Four grains from different samples with ≥3 additional Raman spectra peaks were characterized by high middle to heavy REE values, but they were included in the data set after comparison to other samples indicated that, though high, the values were not unreasonable for those samples.

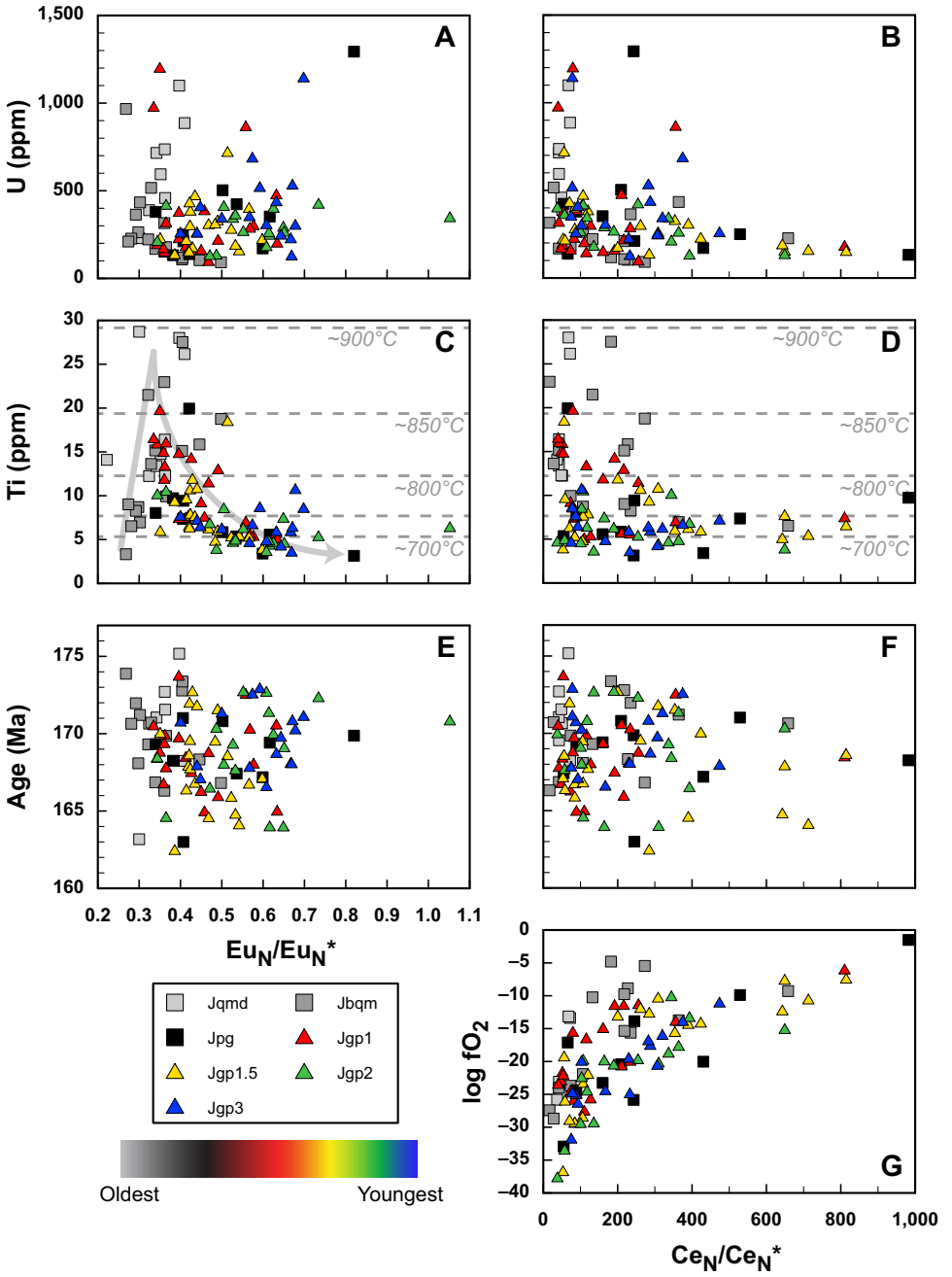


**Figure 6. Zircon trace element and U-Pb age analyses and relevant calculated values for Yerington samples: U versus $Eu_N/Eu_N^*$ (A) and versus $Ce_N/Ce_N^*$ (B); Ti versus $Eu_N/Eu_N^*$ (C) and versus $Ce_N/Ce_N$ (D). Approximate Ti-in-zircon crystallization temperatures calculated using $aSiO_2$ = 1 and $aTiO_2$ = 0.7 using the method of Ferry and Watson (2007). U-Pb zircon age versus $Eu_N/Eu_N^*$ (E) and versus $Ce_N/Ce_N$ (F); (G) Log $fO_2$ versus $Ce_N/Ce_N$. Log $fO_2$ calculated using the method of Trail et al. (2012). Yerington batholith units Jqmd and Jbqm coded in gray; units immediately related to the porphyry dikes coded in black (Jpg, the source of the dike magmas) and colors red to blue, which also correspond to decreasing age order.**

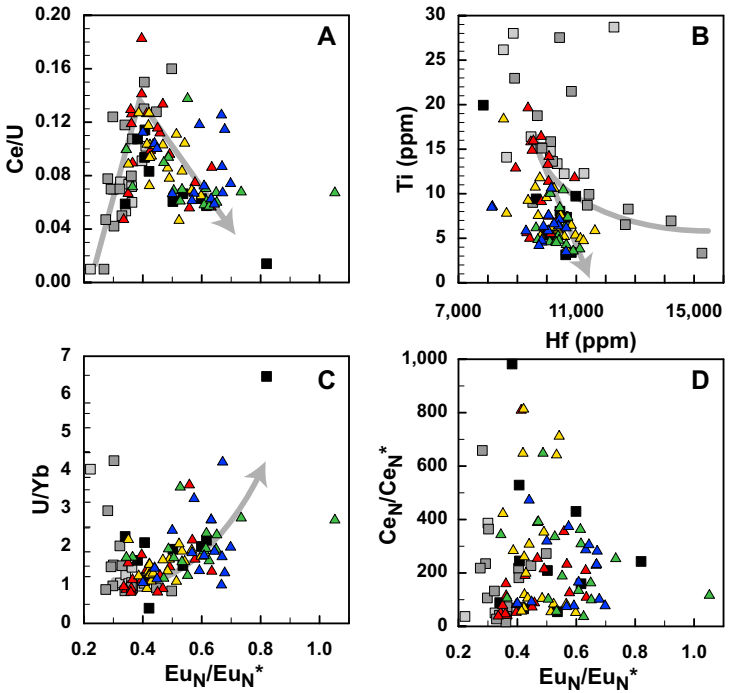


**Figure 7. Yerington zircon trace element analyses. (A) Ce/U versus $Eu_N/Eu_N^*$; (B) Ti versus Hf*; (C) U/Yb versus $Eu_N/Eu_N^*$; (D) $Ce_N/Ce_N^*$ versus $Eu_N/Eu_N^*$. Symbols as in Figure 6.**

One of these grains (Jgp3_6.1) was analyzed for $\delta^{18}O$, and the value, error, and counting statistics were comparable to normal-spectra grain data. U-Pb and/or trace element (TE) analyses from four grains with Raman spectra with additional peak locations and low peak amplitude were not included in the data set due to spurious ages, potential involvement of inclusions, or odd trace element results.

These results suggest that—especially in relatively young, low-U zircon—laser Raman spectroscopy prior to further spot analysis may not be a reliable way to effectively discriminate zircons with radiation damage from those that remain structurally intact. This may be because the laser Raman analytical spot is 5 µm wide with a penetration depth of <1 µm (at 514 nm wavelength), whereas the analytical spots for combined U-Pb and/or trace element (U-Pb/TE) and oxygen isotopes have diameters of 25 µm and penetrate 1–2 µm into the grain. Though we took care to overlap the laser Raman spot completely with the U-Pb/TE spot, a considerable amount (~24/25 of the U-Pb/TE spot area) of material not analyzed via laser Raman was included in the U-Pb/TE analysis. A potential solution to this issue in the future would be to analyze a larger portion of each grain via laser Raman prior to further geochemical analysis, although this would not reveal subsurface metamict areas without using a longer laser beam wavelength.

## Geochemical Implications for Yerington

Yerington is a well-studied magmatic system, but this study differs from previous Yerington research in that we present a suite of zircon ages, trace element, and oxygen isotope data for the rocks exposed in the Yerington mine to investigate if zircon compositional variation is linked with processes that

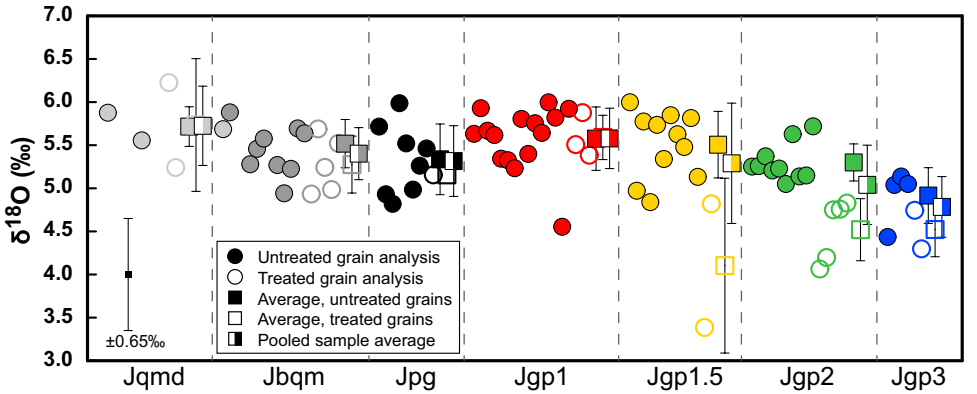


**Figure 8. Oxygen isotope compositions of Yerington zircon. Samples are arranged in order of oldest age (based on field relations; left) to youngest (right). 1σ standard deviation bars are shown on sample averages; 2σ standard error on individual analyses, including analytical error, ranges from ± 0.64 to ± 0.69‰. An example of ± 0.65‰ 2σ SE is illustrated in the bottom left. Symbol colors as in Figures 6 and 7.**

later produced economically important Cu deposits. Dilles et al. (2015) also report similar zircon trace element concentrations for many of the same units sampled outside the Yerington mine.

The evolution of a porphyry magmatic system to produce conditions suitable for Cu to concentrate and produce economic deposits is a chemically multi-phase, multi-step process (e.g., Dilles et al., 2015 and references therein). Based on quartz-hosted melt inclusions from porphyry magmas at Yerington, the timing of Cu-bearing fluid generation is interpreted to be contemporaneous with porphyry dike crystallization (Dilles, 1987). However, zircon crystallization is not concurrent with Cu ore emplacement (Dilles, 1987), and zircon growth may be insufficient during critical changes in conditions leading to ore-fluid generation to be resolvable with current analytical techniques. Our data reflect this in the lack of correlation between $Eu_N/Eu_N^*$ and $Ce_N/Ce_N^*$ in zircon and whole rock Cu concentrations for individual units (Tables 1 and 2; Fig. 7). Moreover, variation in $Ce_N/Ce_N^*$ does not correlate with age or any other measured geochemical attribute and therefore does not appear to record any specific discernible magmatic processes in the Yerington system. Lee (2008) and Lee et al. (2017) reported a similar finding at the El Salvador, Chile porphyry Cu system.

$Eu_N/Eu_N^*$ increases with decreasing Ti (e.g., Dilles et al., 2015; this study), age, and increasing U/Yb in Yerington zircon. For values <0.4, $Eu_N/Eu_N^*$ in Yerington zircon is positively correlated with Ce/, but correlation at values of $Eu_N/Eu_N^*$>0.4 is negative (Fig. 7). This could be a function of changing $D_U^{zrc/melt}$ with temperature (Rubatto and Hermann, 2007; Claiborne et al., 2016)—our data indicate an increase in U by ~4 times as T drops ~150 °C. Alternatively, variations in oxidation conditions are known to affect trace elemental partitioning in zircon for elements with variable charge (e.g., Luo and Ayers, 2009; Burnham and Berry, 2012), and Burnham and Berry (2012) demonstrate that compatibility of U decreases and compatibility of Ce increases as log $fO_2$ rises (i.e., oxidation increases) in a synthetic andesitic melt.

The average Yerington zircon REE pattern is typical for melts associated with porphyry Cu systems and has much higher $Eu_N/Eu_N^*$ than reduced, plagioclase-dominated systems (lunar zircons used as an end-member reduced composition; Taylor et al., 2009) or hydrothermal systems (i.e., highly oxidized; Hoskin et al., 1998) (Fig. 2). Plagioclase is a dominant phase at Yerington and other porphyry Cu systems (e.g., Dilles et al., 2015), as it is in essentially all crustal systems, and its presence complicates the use of the Eu anomaly as purely an indicator of changes in magmatic oxidation conditions. We interpret the lack of correlation between $Eu_N/Eu_N^*$ and $Ce_N/Ce_N^*$ in Yerington zircon to reflect dominance by fractional crystallization, which obscures the influence of oxidation changes. The similarity between zircon compositions in the early McLeod Hill (Jqmd) and Bear (Jbqm) units and the later Luhr Hill granite (Jpg) and porphyry dikes (Jgp) also implies that the Yerington zircon compositions do not reflect changes in oxidation conditions related to Cu mineralization.

Decreasing Ti concentrations in Yerington zircons over time implies a decrease in zircon crystallization temperature (Ferry and Watson, 2007) (Fig. 6). Dilles et al. (2015) noted similar high crystallization temperatures (800–850 °C) for zircons from the McLeod Hill and Bear units that comprise the oldest part of the Yerington batholith, and lower near-eutectic temperatures (~700 °C) for the porphyry dikes and the Luhr Hill granite. However, the Yerington Mine data presented here indicate higher Ti (and therefore T; ~750–850 °C) for Jgp1 zircons than the other porphyry units and the Luhr Hill sample (Jpg). This is significant because Jgp1 is associated with the highest quartz vein density and has the highest Cu grades in and near the dike, indicating a more abundant hydrothermal fluid flux than the other dikes experienced. A noticeable increase in temperatures, Cu, and perhaps volatiles may indicate a deeper and hotter—and by implication, more mafic—source of hydrothermal fluids associated with the Jgp1 dike. There is very little evidence of mafic magmas in the Luhr Hill granite exposures in the Yerington district (e.g., Proffett and Dilles, 1984; Dilles, 1987; and others). Ti concentrations in zircons may therefore provide an additional path to deciphering deeper magmatic processes associated with the Yerington batholith.

$\delta^{18}O$ values between Yerington samples are unresolvable within 2σ error (Fig. 8). Despite petrogenesis in the complicated magmatic regime of an arc environment, Yerington zircon analyses are within error of $\delta^{18}O$ for mantle melt-equilibrated magmatic zircon (5.3 ± 0.3‰; Valley, 2003). Yerington magmas' oxygen isotope composition as measured in fresh rock is 6.7–7.0‰ (Dilles et al., 1992), and fractionation between zircon and rock ($\Delta^{18}O$(zrc-whole rock)) is ~–2‰ for granites (Valley et al., 2005, and references therein). Therefore, we would expect zircons crystallizing from a silicic magma to have $\delta^{18}O$ ~5.0‰ based on the conditions established for Yerington. $\delta^{18}O$ from several individual zircon grains from porphyries Jgp1, 1.5, and 2 is higher than 5.0‰, and $\delta^{18}O$ values from four grains between samples Jgp1.5, 2, and 3 are below this value, indicating that some individual grains crystallized in a slightly lower-$\delta^{18}O$ magma in the later stages of Yerington magmatism. This is somewhat surprising because $\delta^{18}O$ generally increases slightly during differentiation (Taylor and Sheppard, 1986). Strontium isotope values suggest late brines that caused Na-Ca alteration between Jgp2 and Jgp3 intrusion had low $\delta^{18}O$ (Dilles and Farmer, 2001). These fluids—or assimilation of rocks altered by such fluids—may have contributed in minor ways to the magma from which the later porphyries crystallized. Small sample sizes, particularly for Jgp3, prohibit further assessment of the potential role of late-stage, low-$\delta^{18}O$ fluids in the Yerington units examined here. However, this may be an avenue for further research.

Yerington zircon Eu anomalies record a similar shift toward slightly more oxidizing conditions coincident with the drop in zircon crystallization temperature in the youngest and least-mineralized (overall) units (Figs. 6 and 7). Our U-Pb ages are statistically irresolvable at a 2σ level, precluding quantitative assessment of timescales over which host and dike units crystallized, but field relations are well established and allow us to speculate on the involvement of late-stage lower-$\delta^{18}O$ material. Dilles et al. (2015) state that Fe/S in magmas correlates negatively with $fO_2$. Late $SO_2$ degassing, which is a primary driver of Cu ore formation in porphyry systems, involves a decrease in Fe/S and an increase in $fO_2$ (Dilles et al., 2015). Dilles et al. (2015) also report a greater range

of but general increase in $Eu_N/Eu_N^*$ with increasing Hf in zircon from mineralized Yerington samples—a trend not observed in this study when zircons from a suite of host rocks and porphyry dikes is considered.

## CONCLUSIONS

Natural incorporation of tetravalent radioactive elements, such as U and Th, helps make zircon an excellent geochronometer. However, decay of radionuclides results in radiation damage to the crystal structure over time, which enhances diffusivity and thereby can enhance Pb loss and affect isotope ratios and trace element concentrations (e.g., Wang et al., 2014 and references therein). Thermal annealing and chemical abrasion (TA/CA) treatment has been applied to TIMS U-Pb analysis in an effort to remove or minimize damaged (i.e., non-crystalline) areas of zircon and improve precision and accuracy, but there has been limited application of TA/CA treatment for SIMS spot analysis of ages, trace element concentrations, or isotopic compositions. Our results demonstrate that TA/CA treatment of low to moderate-U (90–2200; avg. ~320 ppm U) Jurassic-age zircons prior to analysis does not yield differences that are resolvable within uncertainty in U–Pb age, TE content, or $\delta^{18}O$ as compared to untreated grains, and suggest that TA/CA treatment of zircon should not preclude treated grains from trace element or oxygen isotope analysis on account of the treatment. However, conclusions drawn regarding oxygen isotope analyses are provisional and would strongly benefit from additional analyses to increase sample sizes. Lack of statistically different results from treated and untreated aliquots is likely due to low U content. Our results for Yerington zircon suggest that laser Raman spectroscopy prior to further analysis of relatively young, low-U zircon is not be a reliable way to effectively discriminate zircons because they need to be strongly metamict for laser Raman to be an effective diagnostic tool (cf. >2000 ppm U zircon in Wang et al., 2014).

Our new SHRIMP-RG U-Pb zircon ages agree with the higher precision U-Pb TIMS ages reported by Dilles and Wright (1988) and show little evidence for inheritance. Titanium concentrations (3–29 ppm; avg. 9.8 ± 5.6 (1σ) ppm) decrease and inversely correlate with $Eu_N/Eu_N^*$ (0.19–1.05; avg. 0.45 ± 0.14 (1σ)) and Yb/Gd over time, the latter of which suggests limited fractional crystallization and a decrease in zircon crystallization temperatures in the Yerington Mine magmatic system. Titanium concentrations in zircons and the Ti-in-zircon thermometer may therefore provide an additional path to deciphering deeper magmatic processes associated with the Yerington batholith. Ce/U increases with increasing $Eu_N/Eu_N^*$ in host rock–sourced zircons until $Eu_N/Eu_N^*$~0.4, when ore-bearing porphyry dike–sourced zircons show decreasing Ce/U with increasing $Eu_N/Eu_N^*$, indicating fractional crystallization. The lack of correlation between $Eu_N/Eu_N^*$ and $Ce_N/Ce_N^*$ in Yerington zircon implies that these metrics are not reliable indicators of changes in magmatic oxidation conditions. New oxygen isotope compositions in Yerington porphyry dike zircons, their Luhr Hill granite magmatic source, and the larger Bear and McLeod Hill units of the Yerington batholith are unresolvable within 2σ error and are consistent with previously reported whole rock values.


### ACKNOWLEDGMENTS

We thank John Dilles, an anonymous reviewer, and editor Shanaka de Silva for thorough, thoughtful, and helpful reviews. Financial assistance from a Geological Society of America Southeastern Section grant (TJB) and the Kenan Endowed Chair Research Fund (CFM) funded this research. This work would not have been possible without the support and cooperation of Singatse Peak Services, LLC, Yerington, Nevada. We gratefully acknowledge the contribution of Roland Mundil at Berkeley Geochronology Center for facilitating the TA/CA treatment and for providing intellectual support. Thanks also to Yu Lin at Stanford University for enabling the laser Raman measurements.


### REFERENCES CITED


Baertschi, P., 1976, Absolute $^{18}O$ content of standard mean ocean water: Earth and Planetary Science Letters, v. 31, no. 3, p. 341–344, doi:10.1016/0012-821X(76)90115-1.

Ballard, J.R., Palin, M.J., and Campbell, I.H., 2002, Relative oxidation states of magmas inferred from Ce(IV)/Ce(III) in zircon: Application to porphyry copper deposits of northern Chile: Contributions to Mineralogy and Petrology, v. 144, no. 3, p. 347–364, doi:10.1007/s00410-002-0402-5.

Barth, A.P., and Wooden, J.L., 2010, Coupled elemental and isotopic analyses of polygenetic zircons from granitic rocks by ion microprobe, with implications for melt evolution and the sources of granitic magmas: Chemical Geology, v. 277, no. 1–2, p. 149–159, doi:10.1016/j.chemgeo.2010.07.017.

Black, L.P., Kamo, S.L., Allen, C.M., Davis, D.W., Aleinikoff, J.N., Valley, J.W., Mundil, R., Campbell, I.H., Korsch, R.J., Williams, I.S., and Foudoulis, C., 2004, Improved $^{206}Pb/^{238}U$ microprobe geochronology by the monitoring of a trace-element-related matrix effect; SHRIMP, ID-TIMS, ELA-ICP-MS and oxygen isotope documentation for a series of zircon standards: Chemical Geology, v. 205, no. 1–2, p. 115–140, doi:10.1016/j.chemgeo.2004.01.003.

Burnham, A.D., and Berry, A.J., 2012, An experimental study of trace element partitioning between zircon and melt as a function of oxygen fugacity: Geochimica et Cosmochimica Acta, v. 95, p. 196–212, doi:10.1016/j.gca.2012.07.034.

Carten, R.B., 1986, Sodium-calcium metasomatism; chemical, temporal, and spatial relationships at the Yerington, Nevada, porphyry copper deposit: Economic Geology and the Bulletin of the Society of Economic Geologists, v. 81, no. 6, p. 1495–1519, doi:10.2113/gsecongeo.81.6.1495.

Chelle-Michou, C., Chiaradia, M., Ovtcharova, M., Ulianov, A., and Wotzlaw, J.-F., 2014, Zircon petrochronology reveals the temporal link between porphyry systems and the magmatic evolution of their hidden plutonic roots (the Eocene Coroccohuayco deposit, Peru): Lithos, v. 198, p. 129–140, doi:10.1016/j.lithos.2014.03.017.

Cherniak, D.J., and Watson, E.B., 2003, Diffusion in Zircon: Reviews in Mineralogy and Geochemistry, v. 53, no. 1, p. 113–143, doi:10.2113/0530113.

Cherniak, D.J., Hanchar, J.M., and Watson, E.B., 1997, Diffusion of tetravalent cations in zircon: Contributions to Mineralogy and Petrology, v. 127, no. 4, p. 383–390, doi:10.1007/s004100050287.

Claiborne, L.L., Miller, C.F., Gualda, G.A.R., Fleming, M.A., Covey, A.K., Wooden, J.L., and Carley, T.L., 2016, Zircon as a magma monitor: Robust partition coefficients from surface, rim, and glass measurements from natural systems: Yokohama, Japan, VM Goldschmidt Conference Program with Abstracts, abstract 4756.

Cline, J.S., and Bodnar, R.J., 1991, Can economic porphyry copper mineralization be generated by a typical calc-alkaline melt?: Journal of Geophysical Research, v. 96, no. B5, p. 8113–8126, doi:10.1029/91JB00053.

Colombini, L.L., Miller, C.F., Gualda, G.R., Wooden, J.L., and Miller, J.S., 2011, Sphene and zircon in the Highland Range volcanic sequence (Miocene, southern Nevada, USA): elemental partitioning, phase relations, and influence on evolution of silicic magma: Mineralogy and Petrology, v. 102, no. 1–4, p. 29–50, doi:10.1007/s00710-011-0177-3.

Dawson, P., Hargreave, M.M., and Wilkinson, G.R., 1971, The vibrational spectrum of zircon ($ZrSiO_4$): Journal of Physics. C. Solid State Physics, v. 4, no. 2, p. 240–256, doi:10.1088/0022-3719/4/2/014.

Dilles, J.H., 1987, Petrology of the Yerington Batholith, Nevada: Evidence for evolution of porphyry copper ore fluids: Economic Geology and the Bulletin of the Society of Economic Geologists, v. 82, no. 7, p. 1750–1789, doi:10.2113/gsecongeo.82.7.1750.

Dilles, J.H., and Farmer, G., 2001, Sodium-calcium alteration in the Yerington district, Nevada, due to convection of sedimentary brines, and relation to porphyry Cu and Fe-oxide-Cu (Au)

deposits: Townsville, James Cook University: Economic Geology Research Unit Contribution, v. 59, p. 50–51.
Dilles, J.H., and Wright, J.E., 1988, The chronology of early Mesozoic arc magmatism in the Yerington district of western Nevada and its regional implications: Geological Society of America Bulletin, v. 100, no. 5, p. 644–652, doi:10.1130/0016-7606(1988)100<0644:TCOEMA>2.3.CO;2.
Dilles, J.H., Solomon, G.C., Taylor, H.P., and Einaudi, M.T., 1992, Oxygen and hydrogen isotope characteristics of hydrothermal alteration at the Ann-Mason porphyry copper deposit, Yerington, Nevada: Economic Geology and the Bulletin of the Society of Economic Geologists, v. 87, no. 1, p. 44–63, doi:10.2113/gsecongeo.87.1.44.
Dilles, J.H., Einaudi, M.T., Proffett, J.M., and Barton, M.D., 2000, Overview of the Yerington porphyry copper district: Magmatic to nonmagmatic sources of hydrothermal fluids, their flow paths, alteration effects on rocks, and Cu-Mo-Fe-Au ores, *in* Dilles, J.H., Barton, M.D., Johnson, D.A., Proffett, J.M., and Einaudi, M.T., eds., Contrasting Styles of Intrusion Associated with Hydrothermal Systems: Society of Economic Geologists Guide Book Series, v. 32, part 1, p. 55–66.
Dilles, J.H., Kent, A.J.R., Wooden, J.L., Tosdal, R.M., Koleszar, A., Lee, R.G., and Farmer, L.P., 2015, Zircon compositional evidence for sulfur-degassing from ore-bearing arc magmas: Economic Geology and the Bulletin of the Society of Economic Geologists, v. 110, no. 1, p. 241–251, doi:10.2113/econgeo.110.1.241.
Ferry, J.M., and Watson, E.B., 2007, New thermodynamic models and revised calibrations for the Ti-in-zircon and Zr-in-rutile thermometers: Contributions to Mineralogy and Petrology, v. 154, no. 4, p. 429–437, doi:10.1007/s00410-007-0201-0.
Ghiorso, M.S., and Gualda, G.A.R., 2013, A method for estimating the activity of titania in magmatic liquids from the compositions of coexisting rhombohedral and cubic iron–titanium oxides: Contributions to Mineralogy and Petrology, v. 165, no. 1, p. 73–81, doi:10.1007/s00410-012-0792-y.
Hanchar, J.M., and van Westrenen, W., 2007, Rare Earth Element Behavior in Zircon-Melt Systems: Elements, v. 3, no. 1, p. 37–42, doi:10.2113/gselements.3.1.37.
Hoskin, P.W.O., and Schaltegger, U., 2003, The Composition of Zircon and Igneous and Metamorphic Petrogenesis: Reviews in Mineralogy and Geochemistry, v. 53, no. 1, p. 27–62, doi:10.2113/0530027.
Hoskin, P.W.O., Kinny, P.D., and Wyborn, D., 1998, Chemistry of hydrothermal zircon: Investigating timing and nature of water-rock interaction, *in* Arehart, G., and Hulston, J., eds., Water-Rock Interaction: Rotterdam, AA Balkema, p. 545–548.
Ireland, T.R., and Williams, I.S., 2003, Considerations in Zircon Geochronology by SIMS: Reviews in Mineralogy and Geochemistry, v. 53, no. 1, p. 215–241, doi:10.2113/0530215.
Irmer, G., 1985, On the influence of the apparatus function on the determination of scattering cross sections and lifetime from optical phonon spectra: Experimentalle Technik der Physik, v. 33, p. 501–506 (in German).
Kryza, R., Crowley, Q.G., Larionov, A., Pin, C., Oberc-Dziedzic, T., and Mochnacka, K., 2012, Chemical abrasion applied to SHRIMP zircon geochronology: An example from the Variscan Karkonosze Granite (Sudetes, SW Poland): Gondwana Research, v. 21, no. 4, p. 757–767, doi:10.1016/j.gr.2011.07.007.
Lee, C.-T.A., Luffi, P., Chin, E.J., Bouchet, R., Dasgupta, R., Morton, D.M., Le Roux, V., Yin, Q., and Jin, D., 2012, Copper Systematics in Arc Magmas and Implications for Crust-Mantle Differentiation: Science, v. 336, no. 6077, p. 64 LP-68.
Lee, R.G., 2008, Genesis of the El Salvador Porphyry Copper Deposit, Chile and Distribution of Epithermal Alteration at Lassen Peak, California [Ph.D. thesis]: Corvallis, Oregon, Oregon State University, 322 p.
Lee, R.G., Dilles, J.H., Tosdal, R.M., Wooden, J.L., and Mazdab, F.K., 2017, Magmatic evolution of granodiorite intrusions at the El Salvador porphyry copper deposit, Chile, based on trace element composition and U/Pb age of zircons: Economic Geology and the Bulletin of the Society of Economic Geologists, v. 112, no. 2, p. 245–273, doi:10.2113/econgeo.112.2.245.
Liang, H.-Y., Campbell, I.H., Allen, C., Sun, W.-D., Liu, C.-Q., Yu, H.-X., Xie, Y.-W., and Zhang, Y.-Q., 2006, Zircon $Ce^{4+}/Ce^{3+}$ ratios and ages for Yulong ore-bearing porphyries in eastern Tibet: Mineralium Deposita, v. 41, no. 2, p. 152–159, doi:10.1007/s00126-005-0047-1.
Lidzbarski, M.I., 2014, U-Pb Geochronology of the Miocene Peach Spring Tuff Supereruption and Precursor Cook Canyon Tuff, Western Arizona, USA [M.S. thesis]: San Jose, California, San Jose State University.
Ludwig, K.R., 2009, SQUID 2, A User's Manual: Berkeley Geochronology Center Special Publication, p. 100.
Ludwig, K.R., 2012, Isoplot 3.75, A Geochronological Toolkit for Excel: Berkeley Geochronology Center Special Publication, p. 75.
Luo, Y., and Ayers, J.C., 2009, Experimental measurements of zircon/melt trace-element partition coefficients: Geochimica et Cosmochimica Acta, v. 73, no. 12, p. 3656–3679, doi:10.1016/j.gca.2009.03.027.
Mattinson, J.M., 2005, Zircon U-Pb chemical abrasion ("CA-TIMS") method: Combined annealing and multi-step partial dissolution analysis for improved precision and accuracy of zircon ages: Chemical Geology, v. 220, no. 1–2, p. 47–66, doi:10.1016/j.chemgeo.2005.03.011.
McDonough, W.F., and Sun, S.-s., 1995, The composition of the Earth: Chemical Geology, v. 120, p. 223–253, doi:10.1016/0009-2541(94)00140-4.
McDowell, S.M., Miller, C.F., Mundil, R., Ferguson, C.A., and Wooden, J.L., 2014, Zircon evidence for a ~200 k.y. supereruption-related thermal flare-up in the Miocene southern Black Mountains, western Arizona, USA: Contributions to Mineralogy and Petrology, v. 168, no. 1, p. 1031, doi:10.1007/s00410-014-1031-5.
Mundil, R., Ludwig, K.R., Metcalfe, I., and Renne, P.R., 2004, Age and Timing of the Permian Mass Extinctions: U/Pb Dating of Closed-System Zircons: Science, v. 305, no. 5691, p. 1760–1763, doi:10.1126/science.1101012.
Nasdala, L., Pidgeon, R.T., Wolf, D., and Irmer, G., 1998, Metamictization and U-Pb isotopic discordance in single zircons: A combined Raman microprobe and SHRIMP ion probe study: Mineralogy and Petrology, v. 62, p. 1–27, doi:10.1007/BF01173760.
Pasteris, J.D., 1996, Mount Pinatubo volcano and "negative" porphyry copper deposits: Geology, v. 24, p. 1075–1078, doi:10.1130/0091-7613(1996)024<1075:MPVANP>2.3.CO;2.
Peck, W.H., Valley, J.W., and Graham, C.M., 2003, Slow oxygen diffusion rates in igneous zircons from metamorphic rocks: The American Mineralogist, v. 88, no. 7, p. 1003–1014, doi:10.2138/am-2003-0708.
Proffett, J.M., 1977, Cenozoic geology of the Yerington district, Nevada, and implications for the nature and origin of Basin and Range faulting: Geological Society of America Bulletin, v. 88, no. 2, p. 247–266, doi:10.1130/0016-7606(1977)88<247:CGOTYD>2.0.CO;2.
Proffett, J.M., Jr., 1979, Ore deposits of the western United States: A summary, in Ridge, J.D., ed., Papers on Mineral Deposits of Western North America: Nevada Bureau of Mines and Geology Report 33, p. 13–32.
Proffett, J.M., 2009, High Cu grades in porphyry Cu deposits and their relationship to emplacement depth of magmatic sources: Geology, v. 37, no. 8, p. 675–678, doi:10.1130/G30072A.1.
Proffett, J.M., and Dilles, J.H., 1984, Geologic map of the Yerington district, Nevada: Nevada Bureau of Mines and Geology, Map 77, scale: 1:24,000.
Rubatto, D., and Hermann, J., 2007, Experimental zircon/melt and zircon/garnet trace element partitioning and implications for the geochronology of crustal rocks: Chemical Geology, v. 241, no. 1, p. 38–61, doi:10.1016/j.chemgeo.2007.01.027.
Schoene, B., Crowley, J.L., Condon, D.J., Schmitz, M.D., and Bowring, S.A., 2006, Reassessing the uranium decay constants for geochronology using ID-TIMS U-Pb data: Geochimica et Cosmochimica Acta, v. 70, no. 2, p. 426–445, doi:10.1016/j.gca.2005.09.007.
Stacey, J.S., and Kramers, J.D., 1975, Approximation of terrestrial lead isotope evolution by a two-stage model: Earth and Planetary Science Letters, v. 26, no. 2, p. 207–221, doi:10.1016/0012-821X(75)90088-6.
Streck, M.J., and Dilles, J.H., 1998, Sulfur content of oxidized arc magmas as recorded in apatite from a porphyry copper batholith: Geology, v. 26, p. 523–526, doi:10.1130/0091-7613(1998)026<0523:SEOOAM>2.3.CO;2.
Sun, W., Arculus, R.J., Kamenetsky, V.S., and Binns, R.A., 2004, Release of gold-bearing fluids in convergent margin magmas prompted by magnetite crystallization: Nature, v. 431, no. 7011, p. 975–978, doi:10.1038/nature02972.
Syme, R.W.G., Lockwood, D.J., and Kerr, H.J., 1977, Raman spectrum of synthetic zircon ($ZrSiO_4$) and thorite ($ThSiO_4$): Journal of Physics C: Solid State Physics, v. 10, no. 8, p. 1335–1348, doi:10.1088/0022-3719/10/8/036.
Taylor, H.P., and Sheppard, S.M.F., 1986, Igneous rocks; I, Processes of isotopic fractionation and isotope systematics: Reviews in Mineralogy and Geochemistry, v. 16, no. 1, p. 227–271.
Taylor, D.J., McKeegan, K.D., and Harrison, T.M., 2009, Lu-Hf zircon evidence for rapid lunar differentiation: Earth and Planetary Science Letters, v. 279, p. 157–164, doi:10.1016/j.epsl.2008.12.030.
Trail, D., Watson, E.B., and Tailby, N.D., 2012, Ce and Eu anomalies in zircon as proxies for the oxidation state of magmas: Geochimica et Cosmochimica Acta, v. 97, p. 70–87, doi:10.1016/j.gca.2012.08.032.

Trail, D., Tailby, N.D., Lanzirotti, A., Newville, M., Thomas, J.B., and Watson, E.B., 2015, Redox evolution of silicic magmas: Insights from XANES measurements of Ce valence in Bishop Tuff zircons: Chemical Geology, v. 402, p. 77–88, doi:10.1016/j.chemgeo.2015.02.033.

Ulrich, T., Gunther, D., and Heinrich, C.A., 1999, Gold concentrations of magmatic brines and the metal budget of porphyry copper deposits: Nature, v. 399, no. 6737, p. 676–679, doi:10.1038/21406.

Valley, J.W., 2003, Oxygen isotopes in zircon: Reviews in Mineralogy and Geochemistry, v. 53, no. 1, p. 343–385, doi:10.2113/0530343.

Valley, J.W., Lackey, J.S., Cavosie, A.J., Clechenko, C.C., Spicuzza, M.J., Basei, M.A.S., Bindeman, I.N., Ferreira, V.P., Sial, A.N., King, E.M., Peck, W.H., Sinha, A.K., and Wei, C.S., 2005, 4.4 billion years of crustal maturation: Oxygen isotope ratios of magmatic zircon: Contributions to Mineralogy and Petrology, v. 150, no. 6, p. 561–580, doi:10.1007/s00410-005-0025-8.

von Quadt, A., Gallhofer, D., Guillong, M., Peytcheva, I., Waelle, M., and Sakata, S., 2014, U-Pb dating of CA/non-CA treated zircons obtained by LA-ICP-MS and CA-TIMS techniques: Impact for their geological interpretation: Journal of Analytical Atomic Spectrometry, v. 29, no. 9, p. 1618–1629, doi:10.1039/C4JA00102H.

Wang, X.-L., Coble, M.A., Valley, J.W., Shu, X.-J., Kitajima, K., Spicuzza, M.J., and Sun, T., 2014, Influence of radiation damage on Late Jurassic zircon from southern China: Evidence from in situ measurements of oxygen isotopes, laser Raman, U-Pb ages, and trace elements: Chemical Geology, v. 389, p. 122–136, doi:10.1016/j.chemgeo.2014.09.013.

Watson, E.B., and Cherniak, D.J., 1997, Oxygen diffusion in zircon: Earth and Planetary Science Letters, v. 148, no. 3, p. 527–544, doi:10.1016/S0012-821X(97)00057-5.

Watts, K., Coble, M., Vazquez, J., Colgan, J., John, D., and Henry, C., 2016, Chemical abrasion-SIMS (CA-SIMS) U-Pb dating of zircon from the late Eocene Caetano caldera, Nevada: Chemical Geology, v. 439, p. 139–151, doi:10.1016/j.chemgeo.2016.06.013.

White, L.T., and Ireland, T.R., 2012, High-uranium matrix effect in zircon and its implications for SHRIMP U-Pb age determinations: Chemical Geology, v. 306–307, p. 78–91, doi:10.1016/j.chemgeo.2012.02.025.

Zhang, M., Salje, E.K.H., Farnan, I., Graeme-Barber, A., Daniel, P., Ewing, R.C., Clark, A.M., and Leroux, H., 2000, Metamictization of zircon: Raman spectroscopic study: Journal of Physics Condensed Matter, v. 12, no. 8, p. 1915–1925, doi:10.1088/0953-8984/12/8/333.